Crystal structure of chloroplastic thioredoxin z defines a type-specific target recognition

Théo Le Moigne, Libero Gurrieri, Pierre Crozet, Christophe Marchand, Mirko Zaffagnini, Francesca Sparla, Stéphane Lemaire, Julien Henri

HAL Id: hal-03280204
https://hal.sorbonne-universite.fr/hal-03280204

Submitted on 7 Jul 2021

[Title]
Crystal structure of chloroplastic thioredoxin z defines a type-specific target recognition

[author information]
Théo Le Moigne[1,2,3] (ORCID 0000-0003-2313-3052), Libero Gurrieri[4] (ORCID 0000-0002-3537-2512), Pierre Crozet[1,3,5] (ORCID 0000-0001-5113-2407), Christophe H. Marchand[1,3,6] (ORCID 0000-0002-0729-3841), Mirko Zaffagnini[4] (ORCID 0000-0001-5115-0859), Francesca Sparla[4] (ORCID 0000-0002-2103-4870), Stéphane D. Lemaire[1,3] (ORCID 0000-0001-6442-0547), Julien Henri[1,3],* (ORCID 0000-0003-0772-8881)

1. Sorbonne Université, CNRS, UMR 7238, Institut de Biologie Paris-Seine, Laboratoire de Biologie Computationnelle et Quantitative, 4 place Jussieu F-75005 Paris, France
2. Faculty of Sciences, Doctoral School of Plant Sciences, Université Paris-Saclay, F-91190 Saint-Aubin, France
3. Sorbonne Université, CNRS, UMR 8226, Institut de Biologie Physico-Chimique, Laboratoire de Biologie Moléculaire et Cellulaire des Eucaryotes, 13 rue Pierre et Marie Curie F-75005 Paris, France
4. Department of Pharmacy and Biotechnology, University of Bologna, via Irnerio 42, I-40126 Bologna, Italy
5. Sorbonne Université, Polytech Sorbonne, F-75005 Paris, France
6. CNRS, Institut de Biologie Physico-Chimique, Plateforme de Protéomique, FR 550, 13 rue Pierre et Marie Curie F-75005 Paris, France

* Corresponding author

[running title]
Structure-function analysis of thioredoxin z

[keywords]
Calvin-Benson cycle, photosynthesis, redox post-translational modifications, protein structure, protein-protein interactions, thioredoxins

[corresponding author details]
julien.henri@sorbonne-universite.fr
Laboratoire de Biologie Computationnelle et Quantitative
UMR 7238 Sorbonne Université CNRS
Campus Jussieu
Case courrier 1540
Bât. A - 5ème étage
4, place Jussieu
75005 Paris France
+33(0)1.44.27.66.06

[summary]
Abstract

Thioredoxins (TRXs) are ubiquitous disulfide oxidoreductases structured according to a highly conserved fold. TRXs are involved in a myriad of different processes through a common chemical mechanism. Plant thioredoxins evolved into seven types with diverse subcellular localization and distinct protein targets selectivity. Five TRX types coexist in the chloroplast, with yet scarcely described specificities. We solved the crystal structure of a chloroplastic z-type TRX, revealing a conserved TRX fold with an original electrostatic surface potential surrounding the redox site. This recognition surface is distinct from all other known TRX types from plant and non-plant sources and is exclusively conserved in plant z-type TRXs. We show that this electronegative surface endows TRXz with a capacity to activate the photosynthetic Calvin-Benson cycle enzyme phosphoribulokinase. TRXz distinct electronegative surface thereby extends the repertoire of TRX-target recognitions.

[introduction]
Introduction

Thioredoxins (TRXs) are small ubiquitous disulfide oxidoreductases (Buchanan et al., 2012, Lillig and Holmgren, 2007, Holmgren, 1968, Hall et al., 1971, Gleason and Holmgren, 1981). TRXs fold into a highly conserved and thermostable domain composed of a mixed β-sheet closely surrounded by α-helices and exposing a WC(G/P)PC pentapeptidic motif (Pan and Bardwell, 2006, Holmgren, 1968). Phylogenetic analyses described the history of the TRX fold through four billion years of evolution into the contemporary proteins (Ingles-Prieto et al., 2013, Napolitano et al., 2019). TRXs modify the ternary or quaternary structures of proteins by reducing target disulfide bonds into separate thiols (Holmgren and Morgan, 1976, Blomback et al., 1974). TRXs have also been proposed to be involved in other redox modifications of cysteines by catalyzing denitrosylation, deglutathionylation, or depersulfidation reactions, contributing therefore to redox signaling cascades and metabolic remodeling (Berger et al., 2016, Bedhomme et al., 2012, Benhar et al., 2008, Greetham et al., 2010, Wedmann et al., 2016), as recently reviewed in (Zaffagnini et al., 2019, Zaffagnini et al., 2016). TRXs midpoint redox potential is comprised between -310 and -230 mV at pH 7 (Gonzalez Porque et al., 1970, Watson et al., 2003, Setterdahl et al., 2003, Collin et al., 2003, Hirasawa et al., 1999) with a nucleophilic active site cysteine reacting in the thiolate state ($-S^-$), favored at physiological pH by a local environment determining a cysteine pK_a in the 6.5-7.5 range (Marchand et al., 2019, Roos et al., 2013, Ferrer-Sueta et al., 2011).

The TRX system is recognized as having multiple roles in a myriad of cellular processes and numerous human diseases (Buchanan et al., 2012, Hanschmann et al., 2013, Lee et al., 2013, Toledano et al., 2013). Non-photosynthetic organisms contain a limited number of TRXs reduced by NADPH:thioredoxin reductase (NTR). By contrast, TRXs form a larger multigene family in photosynthetic organisms (21 isoforms in the model plant *Arabidopsis thaliana* and ten in the unicellular green alga *Chlamydomonas reinhardtii*). Phylogenetic analyses grouped TRXs in cytosolic/mitochondrial h-type, mitochondrial o-type and five chloroplastic types (f-, m-, x-, y- and z-types) (Michelet et al., 2006, Balsera et al., 2014). Cytosolic and mitochondrial TRXs are reduced by NTR but chloroplastic TRXs are specifically reduced in the light by ferredoxin:thioredoxin reductase (FTR) which derives electrons from ferredoxin and the photosynthetic electron transfer chain (Balsera et al., 2014, Jacquot et al., 2009, Michelet et al., 2013, Schurmann and Buchanan, 2008, Zaffagnini et al., 2019, Kang et al., 2019). This unique reduction mechanism allows to couple the redox state of TRX to light intensity and to use the chloroplast TRX system as a light-dependent signaling pathway for regulation of cellular metabolism and processes (Perez-Perez et al., 2017). In photoautotrophic organisms, TRXs were originally identified as light-dependent regulators of the Calvin-Benson cycle (CBC), responsible for fixation of atmospheric CO_2 into triose phosphates using energy (ATP) and reducing power (NADPH) produced in the light by the photosynthetic electron transfer chain. Early

studies identified four key enzymes of the CBC as TRX targets: phosphoribulokinase (PRK) (Wolosiuk and Buchanan, 1978b), glyceraldehyde-3-phosphate dehydrogenase (GAPDH) (Wolosiuk and Buchanan, 1978a), fructose-1,6-bisphosphatase (FBPase) (Holmgren et al., 1977) and sedoheptulose-1,7-bisphosphatase (SBPase) (Nishizawa and Buchanan, 1981). These enzymes have a low activity in the dark and are activated upon illumination by the ferredoxin/TRX system because reduction of specific regulatory disulfides by TRX triggers conformational changes that shift the enzyme to a high activity conformation. Besides the CBC, chloroplast TRXs were later recognized as regulators of multiple targets involved in numerous pathways and processes (Lemaire et al., 2007, Zaffagnini et al., 2019). TRXs were especially recognized to provide electrons for the regeneration of major antioxidant enzymes such as peroxiredoxins (Yoshida et al., 2019b, Liebthal et al., 2018, Perez-Perez et al., 2009, Sevilla et al., 2015, Collin et al., 2003, Tarrago et al., 2009, Navrot et al., 2006).

In the microalga *Chlamydomonas reinhardtii* ten TRX isoforms have been identified including six nuclear-encoded chloroplastic TRXs: CrTRXf1, CrTRXf2, CrTRXm, CrTRXx, CrTRXy, and CrTRXz (Balsera et al., 2014, Lemaire et al., 2007, Zaffagnini et al., 2019). Proteomic analyses based on affinity purification chromatography and *in vitro* reconstitution of the cytosolic TRX system allowed the identification of 1053 TRX targets and 1052 putative regulatory sites in Chlamydomonas (Perez-Perez et al., 2017, Lemaire et al., 2004). Among these, all CBC enzymes were identified indicating that they are potential TRX interactors, and direct TRX-dependent activation of CBC enzymes was only demonstrated for PRK (Gurrieri et al., 2019), FBPase (Huppe and Buchanan, 1989), SBPase (Gutle et al., 2016) and phosphoglycerate kinase (PGK) (Morisse et al., 2014). By contrast with land plants, photosynthetic GAPDH from *Chlamydomonas reinhardtii* (CrGAPDH) is not directly regulated by TRX but only indirectly through formation of the $(A_4\text{-GAPDH})_2\text{-CP12}_4\text{-PRK}_2$ complex (Avilan et al., 2012, Trost et al., 2006, Marri et al., 2009). Among the five TRX types present in chloroplasts, only TRXf has been systematically compared to other types and demonstrated to target FBPase (Michelet et al., 2013, Collin et al., 2003), PRK (Marri et al., 2009, Gurrieri et al., 2019), GAPDH in land plants (Marri et al., 2009) and PGK in Chlamydomonas (Morisse et al., 2014). Structural analysis revealed that electrostatic complementarity was the principal driver of TRXf-targets recognition (Bunik et al., 1999, Balmer et al., 2004, Lemaire et al., 2018, de Lamotte-Guery et al., 1991, Mora-Garcia et al., 1998). Besides, TRXs were recently attributed a reciprocal redox function for the oxidation of targets upon light to dark transitions through the action of TrxL2 and 2-Cys peroxiredoxins (Vaseghi et al., 2018, Cejudo et al., 2019, Yoshida et al., 2019a, Yoshida et al., 2019b, Yoshida et al., 2018, Ojeda et al., 2018). Finally, TRXs are involved in a multiplicity of other plastid functions either through their redox capacities (Kang et al., 2019), in the complex redox cellular network (Konig et al., 2012, Yoshida and Hisabori, 2016) or through participation in large supramolecular assemblies (Schroter et al., 2010, Kulczyk et al., 2017).

In *Populus trichocarpa* and in *Arabidopsis thaliana*, TRXz was reported to be reduced by FTR (Chibani et al., 2011, Yoshida and Hisabori, 2017). TRXz can also act as a potential electron acceptor for a special type of chloroplastic TRX named NADPH:thioredoxin reductase C (NTRC) (Yoshida and Hisabori, 2016), TRXf, m, x and y (Bohrer et al., 2012), and interacts with fructokinase-like proteins (FLN1 and FLN2) in *Arabidopsis thaliana* and *Nicotiana benthamiana* (Arsova et al., 2010). TRXz-FLN interaction regulates plastid-encoded polymerase (PEP) (Arsova et al., 2010, Huang et al., 2013). Notably, TRXz reduces plastid redox insensitive protein 2 (PRIN2) cysteine 68 (C68) hetero-molecular disulfides bridge within a homodimer in *Arabidopsis thaliana*, releasing monomeric PRIN2 that activates PEP transcription (Diaz et al., 2018). TRXz redox activity may however be dispensable and TRXz-FLN1 are proposed to be essential components of the PEP complex (Wimmelbacher and Bornke, 2014). TRXz also interacts with *Arabidopsis thaliana* thioredoxin-like MRL7 (Yua et al., 2014) and Temperature-Sensitive Virescent (TSV) protein mediates TRXz interaction with PEP in *Oryza sativa* (Sun et al., 2017). In rice, TRXz was also found to interact with chloroplastic RNA editing enzymes (Wang et al., 2020). Yet, the full set of TRXz targets or interacting partners is still unknown and the corresponding molecular basis for TRXz specificity towards its targets has to be deciphered.

Altogether, it is striking that the very ancient and simple 12-15 kDa TRX fold has evolved into this plethora of functions, suggesting a fine selection of redox properties and specific surface recognitions. In order to gain insights into the molecular functions of chloroplastic z-type TRXz and the physico-chemical basis for its specificity, we solved the high-resolution crystal structure of TRXz from *Chlamydomonas reinhardtii.* This structure is representative of a z-type TRX and unravels a conserved native folding compared to other structurally solved TRXs. Model analysis mapped its redox site and identified the surfaces it exposes for selective protein recognition. TRXz displays electro-complementary surfaces with CrPRK. We show that PRK is indeed activated by TRXz reduction *in vitro*.

[results]
Results

CrTRXz folds as a canonical thioredoxin
Recombinant TRXz from *Chlamydomonas reinhardtii* (CrTRXz) was heterologously expressed in *E. coli* as a 149 amino acids polypeptide (predicted mature protein including residues 56-183 plus the N-terminal affinity tag) and purified to homogeneity by metal-affinity chromatography. Purified CrTRXz was crystallized, the crystals were cryoprotected and submitted to X-ray diffraction for the collection of a complete dataset indexed in space group $P3_221$ and solved by molecular replacement with CrTRXf2 (PDB ID code: 6I1C) as a search model. Model correction and completion up to 116 amino acid residues and one water molecule was refined to R=0.2296 and R_{free}=0.2335 at a resolution of 2.4 Å (Table 1). CrTRXz folds according to the canonical TRX topology (SCOPe entry c.47), *i.e.* a central mixed β-sheet of four strands sandwiched between two pairs of α-helices (Figure 1A and B). The strands order is 2-1-3-4 with strand 3 antiparallel to strands 1, 2 and 4. The succession of secondary structures is as follows: residues 67-76 form helix 1, residues 80-86 strand 1, residues 91-107 helix 2, residues 111-117 strand 2, residues 122-128 helix 3, residues 135-139 strand 3, residues 148-151 strand 4 and residues 156-167 helix 4 (Figure S1). Length of helix 1 is conserved in the eukaryotic branch of TRX evolution since the last eukaryotic common ancestor (Ingles-Prieto et al., 2013). Residues 118-120 were modelled as one turn of a helix 3_{10} with D119 hydrogen bonding with W89 and the unique water molecule of the model. Residues ^{54}HMVI^{57} and ^{61}KVEKIS^{66} of recombinant CrTRXz form an unfolded extension at the amino-terminus of the model, deforming it from an ideal sphere. Residues 58-60 and 170-183 were not built because of a lack of interpretable electron density. Pairwise alignments of equivalent C_α of CrTRXf2 and CrTRXm onto CrTRXz yielded a root mean square deviation (RMSD) of 0.838 Å and 1.356 Å respectively, confirming the close structural similarity between the experimentally solved Chlamydomonas TRX structures (Figure S2). Further alignments with experimentally determined structures from the protein data bank (PDB) revealed also high similarities with *Plasmodium falciparum* TRX2 (PDB identifier 3UL3, RMSD=1.16 Å), resurrected ancestral TRX from inferred last bacterial common ancestor (4BA7, RMSD=1.18 Å), *Bacteroides fragilis* TRXP (3HXS, RMSD=1.19 Å), and with 20 other TRXs with RMSD ≤ 1.30 Å. CrTRXz topology is classical among TRXs.

CrTRXz redox site and environment
Disulfide oxidoreductase activity of TRX relies on a pair of cysteines located at the amino-terminal tip of helix 2 in a conserved motif composed of the WCGPC peptide. The N-terminal active site cysteine (Cys_N) attacks the disulfide bond on a target protein while the second active site cysteine termed Cys_C resolves the intermolecular disulfide bridge to free the reduced target protein and the oxidized TRX. CrTRXz mature sequence possesses two cysteines: Cys_N (C90) and Cys_C (C93) (Figure S1). Both are located at the tip of helix 2 (Figure 2A). Side chain thiols are modelled at 3.1 Å distance in what appears as a reduced state. Nucleophilic C90 displays a 13.56 Å² solvent-accessible area, making it available for redox exchange with a target protein disulfide. The orientation of its thiol group is however unfavorable to thiol electron exchange because it points inwards in the direction of the TRX core. A local rearrangement of loop 88-91 would be required to tumble C90 thiol towards the solvent. Such a

local rearrangement of TRX redox site would partly account for the entropy dependence of target disulfide binding (Palde and Carroll, 2015). In *Escherichia coli* TRX, D26 is buried in the core of the protein where it acts as a base catalyst in the thiol-disulfide interchange reaction (Chivers and Raines, 1997, LeMaster et al., 1997). D31 was confirmed to play the same role in CrTRXh1, and this requires a water molecule for proton exchange (Menchise et al., 2001). CrTRXz also buries D84 at the equivalent position and its carboxyl side chain points in the direction of resolving C93 at a distance of 6.4 Å (Figure 2B). An intermediate water molecule, though not visible at the resolution of our structure, would fit in between at distances favoring hydrogen bonds with D84 and C93 (Figure 2B). P134 at the amino-terminal side of strand 3 faces the redox site at 3.5 Å and 4.6 Å of C93 and C90, respectively. P134 is built in the *cis* conformation. As reported earlier, this *cis*-proline is an important kinetic bottleneck for protein folding (Kelley and Richards, 1987) and is already observed in inferred precambrian TRXs (Gamiz-Arco et al., 2019). Altogether, redox site microenvironment and structural-dependent functional features of TRXs are present and canonical in CrTRXz.

CrTRXz is monomeric

We unexpectedly observed early elution of purified CrTRXz from size-exclusion chromatography, showing an apparent higher molecular weight of the protein when compared to CrTRXf2. The experiment was repeated over two analytical gel filtration matrices (BioSEC3-300 and S6Increase) and the results were confirmed by comparison of distribution coefficients (Kav): $Kav(CrTRXz)_{BioSEC3-300}$ = 0.625 ± 0.005, $Kav(CrTRXf2)_{BioSEC3-300}$ = 0.89; $Kav(CrTRXz)_{S6Increase}$ = 0.611, $Kav(CrTRXf2)_{S6Increase}$ = 0.723 (Figure S3). According to BioSEC3-300 gel filtration calibrated with globular standards, the apparent molecular weight of CrTRXz is 30 ± 5 kDa, approximating twice the molecular weight of a 16 kDa subunit. Consequently, CrTRXz appears as a possible globular homodimer according to analytical size exclusion chromatography.

Analysis of protein interfaces in the crystal packing with PISA (EMBL-EBI) indeed uncovers six direct contact surfaces of 22.4 Å², 98.9 Å², 286.5 Å², 322.1 Å², 437.3 Å² and 812.1 Å² of the asymmetric unit monomer and its closest neighbors. The available surface of a monomer is 6848 Å², hence the largest 812.1 Å² interface covers 12% of CrTRXz surface. This crystallographic A:B dimer is formed by subunit A at positions x,y,z and subunit B at positions -x+2,-x+y+1,-z+2/3 in a neighboring unit cell (Figure 3A). PISA computes a solvation free energy gain ($\Delta^i G$) of -11.3 kcal.mol^{-1} upon formation of the interface. 21 residues are located at the interface. Ten residues form hydrogen bonds between $R77_A:E71_B$, $R149_A:M127_B$, $E71_A:R77_B$, $M127_A:R149_B$, and at equivalent yet non-symmetrical positions $R129_A:R129_B$. Four residues form multiple salt bridges between $R77_A:E71_B$ and equivalent $E71_A:R77_B$. Overall, PISA scores this interface with a complexation significance to 1 (stable assembly), while the other five detected interfaces score at 0 (no stable assembly).

To try and probe the quaternary structure of CrTRXz in solution, we submitted two independent preparations of pure CrTRXz to small-angle X-rays scattering coupled to size-exclusion chromatography (SEC-SAXS) (Figure 3B,C). Guinier analyses radii of gyration of 20.16 ± 0.25 Å (protein preparation 1) and 23.34 ± 0.43 Å (preparation 2) allowed computation of respective molecular weights intervals of 15.80-17.75 kDa and 18.35-20.85 kDa at a credibility probability higher than 95%. The oligomeric state of CrTRXz detected by SAXS is consequently that of a monomer of 16.2 kDa. Analysis of CrTRXz by mass spectrometry under native or denaturant conditions showed only the presence of monomeric species in our experimental conditions suggesting that in solution CrTRXz is mainly monomeric.

In conclusion, the dimerization observed in crystal packing is too weak or too transitory to represent the principal protein population *in vitro* in the SAXS and MS experimental setups, while the higher apparent molecular weight on size exclusion chromatography may be due to non-globularity. The monomeric state is the most probable form expected in the diluted, non-crystalline physiological context.

CrTRXz reactive surface displays a unique electronegative potential

Multiplicity of TRX types in the chloroplast stroma raises the question of their specificity and the underlying physico-chemical determinants for selective and non-overlapping disulfide bond

recognition in different targets (Lemaire et al., 2007). In order to identify z-type specificities, we analyzed the high-resolution crystal structure of CrTRXz. The secondary structure topology is almost identical to other known TRXs (Figure S2). The redox residues are also positioned at the canonical sites and they form the most conserved surface of the protein among homologs (Figure 1E and 1F) (Ashkenazy et al., 2016). The dynamics of the main chain is approximated by the crystallographic b-factors, the highest values of which are grouped at the amino- and carboxy-terminal ends and at the loop connecting strands 3 and 4 (Figure 1G and 1H). Helices 3 and 1 also group higher than average b-factors, albeit to a lower extent than the aforementioned loop and N/C-termini. This local flexibility may predict functional deformations of CrTRXz structure upon folding, binding of protein partners, or during allosteric controls. All dynamic elements are however located far from the redox site and they are unlikely to contribute alone to the selectivity of CrTRXz towards targets.

The principal determinant of CrTRXf2 selectivity was described as an electropositive crown of residues exposed at the surface surrounding the redox site (Balmer et al., 2004, Bunik et al., 1999, Lemaire et al., 2018, Yokochi et al., 2019). We compared the electrostatic surface of CrTRXz and observed large electronegative patches, and a general lack of electropositive elements (Figure 1C and 1D). Notably, CrTRXz presents the z-type conserved apolar L94 immediately after the redox site WCGPC, while all other plastidial TRX possess in this position either a positively charged residue (R/K for m-, x- and f-type) or an hydrogen bond donor residue (Q for y-type). Differential electrostatic repartition is particularly marked in the vicinity of the redox site and represents a significant qualitative difference with CrTRXf2 and CrTRXm equivalent surfaces (Figure 4B, 4D and 4F). The principal determinants of CrTRXf2 selectivity were proposed to be K78, K114, N130, K131, N133, K134, K143 and K164 (PDB entry 6I1C numbering (Lemaire et al., 2018)). Equivalent positions on structurally aligned CrTRXz are occupied by E63, Q102, D119, E120, N121, P122, Q131 and E151. Seven out of these eight residues are conserved in TRXz homologs (Figure S1) and the electronegative surface is predicted conserved in a land plant ortholog (Figure S4), supporting an important function for type-z physiological functions in plants. In both CrTRXf2 and CrTRXz crystal structures, the aforementioned side chains are located at the protein surfaces and point their polar groups to the solvent. If the amine group of lysines expose a +1 charge while the carboxyl group of aspartates and glutamates expose a -1 charge at physiological pH, aforementioned CrTRXf2 selectivity surface will accumulate a net charge of +6 while corresponding positions on CrTRXz sum a net charge of -4. The contributions of asparagine and glutamine residues to each selectivity surfaces are less explicit since they potentially behave as hydrogen bond donors or acceptors.

Overall, TRXz and TRXf2 recognition modes probably rely on distinct surface properties of targets because they present opposite electrostatic profiles. According to their mature sequence, CrTRXz presents an acidic isoelectric point while that of CrTRXf2 is basic (4.55 and 8.45, respectively). CrTRXm also presents an acidic isoelectric point (5.09), but important surface differences with CrTRXz stem from the charges repartition around the redox surface (Figures 4B and 4D).

TRXz is electro-complementary to known protein interactants

Four candidate proteins are described as TRXz interactants in *Arabidopsis thaliana*: FLN1, FLN2, PRIN2 and MRL7(Yua et al., 2014, Arsova et al., 2010, Diaz et al., 2018). The molecular structure of these proteins is not experimentally determined but their structures were predicted by homology using the PHYRE software (Kelley et al., 2015) (Figure 5). AtFLN1 possesses five cysteines and based on the protein model, adjacent C105 and C106 are buried within the structure and seems to be affected by TRX only in a solvent exposed unfolded state. C204, C398 and C418 are predicted to be solvent-exposed and available for TRX redox interaction (Figure 5A) even though they probably do not form intramolecular disulfide bridges as they appear too distant. C398 is surrounded by an electropositive surface complementary to CrTRXz recognition surface (Figure 5B). Homology-modelled AtFLN2 includes nine cysteines, consecutive C208 and C209 are also located under the surface and probably not accessible in the folded state (Figure 5C). C290, C307, C322, C326, C419 are present at the predicted surface while C529 hidden to solvent and C253 is at the bottom of a deep and narrow cleft. C290, C322, C326 and C327 are surrounded by electropositive surfaces that qualifies them as potential

targets of TRXz redox interaction (Figure 5D). The three later would make good candidates for intra-molecular dithiol/disulfide exchange since their thiols are predicted at 7.7, 8.5 and 9.2 Å distances. AtMRL7 model encompasses two cysteines, both predicted at the solvent exposed surface of the protein (Figure 5E). C281 is surrounded by marked electropositive potentials and may then be targeted by electro-complementary TRXz redox surface (Figure 5F). AtPRIN2 could not be modelled by PHYRE as a globular structure, because of the lack of close homology with experimental models (best sequence identity 27 % over 32 % residue coverage, or 22 % identity for 49 % coverage). However, the 20-residues peptide NH_3^+-LSSLSRRGFV$\underline{C}$RAAEYKFPDP-COO^- centered on redox target C68 (underlined) contains three arginines and one lysine and even though the mature protein sequence confers an acidic pI (4.43), the local environment of the cysteine in this peptide presents a basic pI of 9.31 that would make it a reasonable target for interaction with TRXz electronegative surface.

CrTRXz can activate CrPRK in vitro
While CrPRK is a well-known CrTRXf2 target, presumably because of its partially negative surface around C55, another large positive patch is also present near C55 at the enzymatic pocket (Marri et al., 2009, Gurrieri et al., 2019) . The mixed environment of CrPRK C55 suggests an independent, alternative mechanism of redox activation by TRXz. We probed the activation efficiency of the CrTRXf2, CrTRXz, and CrTRXm on PRK activity. The ability of CrTRXs to reductively activate oxidized CrPRK was measured using different TRX:PRK ratios and assaying the enzyme activity after 1 h of incubation (Figure 6). In every incubation, CrPRK was 5 μM and TRX varies from 0.5 μM (ratio 1:10 TRX:PRK) to 50 μM (ratio 10:1 TRX:PRK). At the lowest ratio (1:10) no TRX significantly activated PRK, while at higher ratios both CrTRXz and CrTRXf2 activated the enzyme. The CrTRXz activation plateaued at 2-fold excess, reaching 60% of maximal activity. No further activation was observed at higher TRX:PRK molar ratios. PRK activity in the presence of CrTRXf2 increased until 6-fold excess, where 100% of maximal activity was obtained. CrTRXm was able to partially activate PRK only at the highest molar ratios (*i.e.* 6:1 and 10:1 TRX:PRK ratios). These results demonstrate that CrTRXf2 is the main activator for PRK *in vitro*, whereas CrTRXz is able to activate CrPRK to a lesser extent.

[discussion]
Discussion

Here, we report the experimental structure of a TRXz from the model eukaryotic alga *Chlamydomonas reinhardtii* (PDB ID code: 7ASW). Structural analysis reveals that chloroplastic CrTRXz is a classical TRX with an atypical electronegative surface conserved in plant homologs. We dissected TRXz surface properties to assess its putative specificity over known target proteins of AtTRXz. Moreover, based on structural features, we proposed the Calvin-Benson enzyme CrPRK as being recognized by CrTRXz, which was confirmed by our *in vitro* activity assays.

CrTRXz maintains the canonical fold of thioredoxin
The determination of the crystal structure of chloroplastic TRXz from the green alga *Chlamydomonas reinhardtii* confirmed that it folds as a canonical αβα compact domain exposing the conserved WCGPC redox pentapeptide at nucleophile attacking distance of incoming target disulfide bond. Other signatures of reactivity and folding were observed in our structure, *e.g.* the base catalyst aspartate in a water-bridging distance to resolving Cys_C, the ten-residue helix 1 of eukaryotic TRXs and the folding bottleneck *cis*-P134. The reactive Cys redox pair appears dissociated in a dithiol state available for the reduction of a target disulfide bond.

CrTRXz evolved distinct features
Although conform to the thioredoxin standard, our crystal structure reveals distinct features on CrTRXz. The peptide connecting strand 2 and helix 3 is folded as a short helix 3_{10} that is stabilized by hydrogen-bonding interaction of D119 with W89, adjacent to Cys_N in the redox site. This particular

state may modify the reactivity of TRXz active site or rather a functional conformation of TRX since D119 is conserved in CrTRXx, y, h1, h2, and o while it is substituted by an isosteric asparagine in CrTRXf2 and m. C126 of AtTRXf1 was shown to be glutathionylated and the glutathionylation demonstrated to subsequently affect the redox capacity of this TRX (Michelet et al., 2005). CrTRXf1 and f2 but not the other TRX types possess this regulatory cysteine, at the first position after aforementioned D119 and its equivalents. Hence, regulation of thioredoxin by redox signaling may be caused by distal effects on the redox site through a bonding network similar to CrTRXz D119-W89. Interestingly, selective inactivation of TRXf by glutathionylation would leave TRXz as an alternative to perform photosynthetic functions such as light- and TRX-dependent activations of PRK.

CrTRXz crystallizes as a homodimer and elutes as larger than globular monomer objects as judged by size-exclusion chromatography. Small-angle X-rays scattering (SAXS) and native mass spectrometry however unequivocally contradicted the dimer hypothesis in solution, with the measured gyration radii and diffusion curves revealing a monomeric state of globular CrTRXz *in vitro*. Dimerization is either a pure crystallization artifact or a transitory interaction in restricted conditions of high local concentration, like those of a liquid-liquid phase separation or of a multiprotein complex. The interaction surface is distant from the redox site and may rather serve to scaffold TRXz-containing complexes with internal two-fold symmetries. Other TRX quaternary states were tested in the past and proved monomeric (Capitani and Schurmann, 2004, Gronenborn et al., 1999) in reduced state (Weichsel et al., 1996).

Electronegativity as a driver of CrTRXz specific complexation
Western blot protein quantification of *Arabidopsis thaliana* leaf extracts indicated relative abundances of 69.1% TRXm, 22.2% TRXf, 6.3% TRXx, 1.3% TRXy and 1.1% TRXz, representing a TRXz concentration of 1-5 pmol.mg^{-1} stromal protein (Okegawa and Motohashi, 2015). Notwithstanding its relative scarcity, TRXz still makes significant contributions to chloroplast functions as demonstrated by the lethality of its deletion mutant. We propose that TRXz loss cannot be compensated by other TRXs because of the irreplaceable specialization of its electronegative surface. Described determinants of TRXf2 selectivity present an opposite, electropositive character compared to TRXz. Reported targets of TRXz in *Arabidopsis thaliana* present exposed cysteines on electropositive surfaces that match TRXz redox site (Figure 5). One interesting candidate for interaction is TRXf itself, since the electropositive environment of its active site is an ideal electro-complementary platform for TRXz docking. Consistently, TRXz was reported to be reduced *in vitro* by FTR (Chibani et al., 2011) but also by other TRX types (Bohrer et al., 2012) suggesting that it could play a specific role in reductive or oxidant signaling (Bohrer et al., 2012, Yoshida and Hisabori, 2016).

We report here that CrTRXz is able to activate CrPRK, a known target of the main CBC activator TRXf2. CrTRXz activation is slightly weaker than that of CrTRXf2 but stronger than CrTRXm activation. It relies on the ratio between TRX and target, so TRXz could efficiently activate PRK or other targets when it reaches a certain concentration in the chloroplast. Interestingly, the cell has at its disposal two different TRXs to activate PRK and tune the CBC flux according to environmental conditions. In conditions when TRXf2 is inactivated by glutathionylation (Michelet et al., 2005), one can hypothesize that TRXz becomes the replacement activator of PRK.

TRX complementarities should now be confirmed by the description of the actual complexes between TRX and targets, ideally from experimental structures at atomic resolution. TRXm, x, and y in the chloroplast still await a comprehensive description of the molecular basis for specific disulfide targeting, as well as TRXh/TRXo and bacterial TRX in their respective compartments. Later on, a global simulation of electron transfers in the proteome will require knowledge on the concentrations of all TRXs, reductant sources, and targets, their mutual binding affinities, interaction turnovers and their cysteine redox potentials.

[methods]

Material and methods

Cloning
Nuclear encoded amino acid sequence of *Chlamydomonas reinhardtii* thioredoxin z (UniRef100 entry A8J0Q8, thioredoxin-related protein ClTRX) was analyzed by TargetP2.0 (Emanuelsson et al., 2007, Almagro Armenteros et al., 2019), ChloroP (Emanuelsson et al., 1999) and Predalgo (Tardif et al., 2012) to predict the transit peptide cutting site and the subsequent mature sequence of chloroplastic protein. The sequence coding for amino acids 56-183 was PCR-amplified from *Chlamydomonas reinhardtii* EST database plasmid AV642845 with DNA primers 5'-TGTCGC**CATATG**GTCATTAGCCATGGAAAG-3' and 5'-CTCCTT**AAGCTT**CTACTGCTGCGGCGCCTCGGG-3'. The PCR product was inserted into pET28a by restriction with NdeI and HindIII and subsequent ligation, yielding pET28a-His$_6$-CrTRXz. Recombinant protein is a fusion of Met-HHHHHH-SSFLVPRGSHM- and TRXz residues 56 to 183, as validated by plasmid Sanger sequencing. Residue numbering is accorded to UniProt sequence A8J0Q8-1 throughout the text.

Expression and purification
Escherichia coli strain BL21(DE3) Rosetta-2 pLysS (Novagen Merck, Darmstadt Germany) was transformed with pET28a-His6-CrTRXz and grown in 1 L of 2YT medium supplemented with kanamycin (50 µg.mL^{-1}) and chloramphenicol (34 µg.mL^{-1}) to exponential phase at an optical density of 0.6 before T7-RNA polymerase induction of overexpression with 200 µmol.L^{-1} IPTG for 3.5 h at 37°C. 4.1 g of cell pellet were resuspended in 20 mL buffer A (20 mmol.L^{-1} Tris-Cl pH 7.9, 200 mmol.L^{-1} NaCl), lysed by 2 min sonication with 0.4 sec pulses at output 5 on W-375 sonicator equipped with microtip (Qsonica, Newtown CT USA) on ice. Total extract was clarified by 20 min centrifugation at 30,000 rcf at 4°C and the soluble fraction was loaded on affinity chromatography over 5 mL of NiNTA resin (Sigma-Aldrich Merck, Darmstad Germany). Resin was step-washed with 10 mL of buffer A supplemented with 10, 20, 30, 40 or 50 mmol.L^{-1} imidazole. Elution was executed with steps of 10 mL of buffer A supplemented with 100, 150, 200 or 250 mmol.L^{-1} imidazole. Collected fractions were analyzed by Coomassie stained SDS-PAGE that revealed the presence of >99 % pure TRXz in wash fractions 20, 30, 40 and 50 and elution fractions 100 and 200. Pooled fractions were buffer exchanged to buffer A and concentrated by ultrafiltration on 3000 MWCO Amicon filter units (Millipore Merck, Darmstadt Germany). A final concentration of 10.2 mg.mL^{-1} was measured by NanoDrop 2000 spectrophotometer (Thermo Fisher Scientific, Waltham MA USA) with theoretical Mw = 16,191.5 g.mol^{-1} and ε_{280} = 5,567.5 mol^{-1}.L.cm^{-1}.

Size-exclusion chromatography
0.1 mg affinity-purified recombinant CrTRXz was loaded on Superose6 10/300 Increase column or BioSEC3-300 column in 20 mmol L^{-1} Tris-Cl pH=7.9, 100 mmol.L^{-1} NaCl. Isocratic elution was recorded at 280 nm.

Small angle X-rays scattering
Diffusion curves were collected from BioSEC3-300 size-exclusion chromatography in line with X-ray exposure capillary at beamline SWING of synchrotron SOLEIL (Saint-Aubin, France). Data were processed with FOXTROT (Xenocs, Grenoble France) using CLEVERAVG algorithms and interpreted with ATSAS (Petoukhov et al., 2012, Franke et al., 2017).

Crystallization and structure determination
Purified CrTRXz was tested for crystallization on commercial sparse-screening conditions (Qiagen, Hilden Germany) of the Joint Center for Structural Genomics screens (Lesley and Wilson, 2005) with a mixture of 30 nL protein and 30 nL precipitant equilibrated against a reservoir volume of 30 µL mother liquor. 30 µm sided monocrystals grew in one week in condition 38 at position D2 of screen IV (0.1 mol.L^{-1} HEPES pH=7,5; 1,26 mol.L^{-1} ammonium sulfate). Crystals were transferred in mother liquor supplemented with 12.5% glycerol and flash-frozen in liquid nitrogen for diffraction experiments at

micro-focused beamline PROXIMA-2A at SOLEIL synchrotron (Saint-Aubin, France). A 99.36 % complete dataset was collected at 2.444 Å resolution. Data was indexed in space group $P3_221$, integrated, scaled and converted with XDSME (Legrand, 2017). Structure was phased by molecular replacement with PHENIX (Adams et al., 2010, Adams et al., 2011) PHASER-MR (McCoy et al., 2007) using CrTRXf2 (PDB 6I1C (Lemaire et al., 2018)) as a search model and a single protein in the asymmetric unit. Model was refined by iterative cycles of manual building in COOT (Emsley and Cowtan, 2004, Emsley et al., 2010) followed by refinement with PHENIX.REFINE (Afonine et al., 2012) until completion of a structure passing MOLPROBITY (Chen et al., 2010) evaluation with 100 % residues in Ramachandran restrains, RMS(bonds)=0.010, RMS(angles)=1.44 and final R_{work}=0.2296, R_{free}=0.2335 (Table 1). Structure representations were drawn with PYMOL (Schrodinger, New York USA).

Thioredoxin activation assay
Chlamydomonas reinhardtii phosphoribulokinase (CrPRK) was recombinantly expressed as published earlier (Gurrieri et al., 2019). Pure CrPRK was oxidized in presence of 0.2 mM 5,5'-dithiobis(2-nitrobenzoic acid) (DTNB, Sigma-Aldrich) for 45 min at room temperature. CrPRK was desalted to stop the oxidation and used to assay TRX activation efficiency. Oxidized CrPRK at 5 µM was incubated in presence of 0.2 mM dithiothreithol (DTT) and from 0.5 µM to 50 µM CrTRXz, CrTRXf2 and CrTRXm for 60 minutes, then PRK activity was assayed as in (Gurrieri et al., 2019). Control activity was obtained incubating CrPRK with 0.2 mM DTT for 60 min. Activities were normalized on fully reduced PRK obtained after 4 h incubation at room temperature in presence of 40 mM DTT.

[data availability statement]
Structural data
Validated crystallographic reflection data and model are deposited in the protein data bank under access code 7ASW.

[author contributions]
Author contributions
Conception, M.Z., F.S., S.D.L., and J.H.; acquisition and analysis of data, T.L.M., L.G., C.H.M., and J.H.; manuscript writing, reviewing and editing, T.L.M., L.G., P.C., C.H.M., M.Z., F.S., S.D.L., and J.H.; funding and resource acquisition, F.S., S.D.L., and J.H. All authors have read and agreed to the final version of the manuscript.

[conflict of interest statement]
Conflict of Interest Statement
The authors have no conflicts of interest to declare.

[references]
References

ADAMS, P. D., AFONINE, P. V., BUNKOCZI, G., CHEN, V. B., DAVIS, I. W., ECHOLS, N., HEADD, J. J., HUNG, L. W., KAPRAL, G. J., GROSSE-KUNSTLEVE, R. W., MCCOY, A. J., MORIARTY, N. W., OEFFNER, R., READ, R. J., RICHARDSON, D. C., RICHARDSON, J. S., TERWILLIGER, T. C. & ZWART, P. H. 2010. PHENIX: a comprehensive Python-based system for macromolecular structure solution. *Acta Crystallogr D Biol Crystallogr,* 66**,** 213-21.

ADAMS, P. D., AFONINE, P. V., BUNKOCZI, G., CHEN, V. B., ECHOLS, N., HEADD, J. J., HUNG, L. W., JAIN, S., KAPRAL, G. J., GROSSE KUNSTLEVE, R. W., MCCOY, A. J., MORIARTY, N. W., OEFFNER, R. D., READ, R. J., RICHARDSON, D. C., RICHARDSON, J. S., TERWILLIGER, T. C. & ZWART, P. H. 2011. The Phenix software for automated determination of macromolecular structures. *Methods,* 55**,** 94-106.

AFONINE, P. V., GROSSE-KUNSTLEVE, R. W., ECHOLS, N., HEADD, J. J., MORIARTY, N. W., MUSTYAKIMOV, M., TERWILLIGER, T. C., URZHUMTSEV, A., ZWART, P. H. & ADAMS, P. D. 2012. Towards automated crystallographic structure refinement with phenix.refine. *Acta Crystallogr D Biol Crystallogr,* 68**,** 352-67.

ALMAGRO ARMENTEROS, J. J., SALVATORE, M., EMANUELSSON, O., WINTHER, O., VON HEIJNE, G., ELOFSSON, A. & NIELSEN, H. 2019. Detecting sequence signals in targeting peptides using deep learning. *Life Sci Alliance,* 2.

ARSOVA, B., HOJA, U., WIMMELBACHER, M., GREINER, E., USTUN, S., MELZER, M., PETERSEN, K., LEIN, W. & BORNKE, F. 2010. Plastidial thioredoxin z interacts with two fructokinase-like proteins in a thiol-dependent manner: evidence for an essential role in chloroplast development in Arabidopsis and Nicotiana benthamiana. *Plant Cell,* 22**,** 1498-515.

ASHKENAZY, H., ABADI, S., MARTZ, E., CHAY, O., MAYROSE, I., PUPKO, T. & BEN-TAL, N. 2016. ConSurf 2016: an improved methodology to estimate and visualize evolutionary conservation in macromolecules. *Nucleic Acids Res,* 44**,** W344-50.

AVILAN, L., PUPPO, C., ERALES, J., WOUDSTRA, M., LEBRUN, R. & GONTERO, B. 2012. CP12 residues involved in the formation and regulation of the glyceraldehyde-3-phosphate dehydrogenase-CP12-phosphoribulokinase complex in Chlamydomonas reinhardtii. *Mol Biosyst,* 8**,** 2994-3002.

BAKER, N. A., SEPT, D., JOSEPH, S., HOLST, M. J. & MCCAMMON, J. A. 2001. Electrostatics of nanosystems: application to microtubules and the ribosome. *Proc Natl Acad Sci U S A,* 98**,** 10037-41.

BALMER, Y., KOLLER, A., VAL, G. D., SCHURMANN, P. & BUCHANAN, B. B. 2004. Proteomics uncovers proteins interacting electrostatically with thioredoxin in chloroplasts. *Photosynth Res,* 79**,** 275-80.

BALSERA, M., UBEREGUI, E., SCHURMANN, P. & BUCHANAN, B. B. 2014. Evolutionary development of redox regulation in chloroplasts. *Antioxid Redox Signal,* 21**,** 1327-55.

BEDHOMME, M., ADAMO, M., MARCHAND, C. H., COUTURIER, J., ROUHIER, N., LEMAIRE, S. D., ZAFFAGNINI, M. & TROST, P. 2012. Glutathionylation of cytosolic glyceraldehyde-3-phosphate dehydrogenase from the model plant Arabidopsis thaliana is reversed by both glutaredoxins and thioredoxins in vitro. *Biochem J,* 445**,** 337-47.

BENHAR, M., FORRESTER, M. T., HESS, D. T. & STAMLER, J. S. 2008. Regulated protein denitrosylation by cytosolic and mitochondrial thioredoxins. *Science,* 320**,** 1050-4.

BERGER, H., DE MIA, M., MORISSE, S., MARCHAND, C. H., LEMAIRE, S. D., WOBBE, L. & KRUSE, O. 2016. A Light Switch Based on Protein S-Nitrosylation Fine-Tunes Photosynthetic Light Harvesting in Chlamydomonas. *Plant Physiol,* 171**,** 821-32.

BLOMBACK, B., BLOMBACK, M., FINKBEINER, W., HOLMGREN, A., KOWALSKA-LOTH, B. & OLOVSON, G. 1974. Enzymatic reduction of disulfide bonds in fibrin-ogen by the thioredoxin system. I. Identification of reduced bonds and studies on reoxidation process. *Thromb Res,* 4**,** 55-75.

BOHRER, A. S., MASSOT, V., INNOCENTI, G., REICHHELD, J. P., ISSAKIDIS-BOURGUET, E. & VANACKER, H. 2012. New insights into the reduction systems of plastidial thioredoxins point out the unique properties of thioredoxin z from Arabidopsis. *J Exp Bot,* 63**,** 6315-23.

BUCHANAN, B. B., HOLMGREN, A., JACQUOT, J. P. & SCHEIBE, R. 2012. Fifty years in the thioredoxin field and a bountiful harvest. *Biochim Biophys Acta,* 1820**,** 1822-9.

BUNIK, V., RADDATZ, G., LEMAIRE, S., MEYER, Y., JACQUOT, J. P. & BISSWANGER, H. 1999. Interaction of thioredoxins with target proteins: role of particular structural elements and electrostatic properties of thioredoxins in their interplay with 2-oxoacid dehydrogenase complexes. *Protein Sci,* 8**,** 65-74.

CAPITANI, G. & SCHURMANN, P. 2004. On the Quaternary Assembly of Spinach Chloroplast Thioredoxin m. *Photosynth Res,* 79**,** 281-5.

CEJUDO, F. J., OJEDA, V., DELGADO-REQUEREY, V., GONZALEZ, M. & PEREZ-RUIZ, J. M. 2019. Chloroplast Redox Regulatory Mechanisms in Plant Adaptation to Light and Darkness. *Front Plant Sci,* 10**,** 380.

CHEN, V. B., ARENDALL, W. B., 3RD, HEADD, J. J., KEEDY, D. A., IMMORMINO, R. M., KAPRAL, G. J., MURRAY, L. W., RICHARDSON, J. S. & RICHARDSON, D. C. 2010. MolProbity: all-atom structure validation for macromolecular crystallography. *Acta Crystallogr D Biol Crystallogr,* 66**,** 12-21.

CHIBANI, K., TARRAGO, L., SCHÜRMANN, P., JACQUOT, J. P. & ROUHIER, N. 2011. Biochemical properties of poplar thioredoxin z. *FEBS Lett,* 585.

CHIVERS, P. T. & RAINES, R. T. 1997. General acid/base catalysis in the active site of Escherichia coli thioredoxin. *Biochemistry,* 36**,** 15810-6.

COLLIN, V., ISSAKIDIS-BOURGUET, E., MARCHAND, C., HIRASAWA, M., LANCELIN, J. M., KNAFF, D. B. & MIGINIAC-MASLOW, M. 2003. The Arabidopsis plastidial thioredoxins: new functions and new insights into specificity. *J Biol Chem,* 278**,** 23747-52.

DE LAMOTTE-GUERY, F., MIGINIAC-MASLOW, M., DECOTTIGNIES, P., STEIN, M., MINARD, P. & JACQUOT, J. P. 1991. Mutation of a negatively charged amino acid in thioredoxin modifies its reactivity with chloroplastic enzymes. *Eur J Biochem,* 196**,** 287-94.

DIAZ, M. G., HERNANDEZ-VERDEJA, T., KREMNEV, D., CRAWFORD, T., DUBREUIL, C. & STRAND, A. 2018. Redox regulation of PEP activity during seedling establishment in Arabidopsis thaliana. *Nat Commun,* 9**,** 50.

EMANUELSSON, O., BRUNAK, S., VON HEIJNE, G. & NIELSEN, H. 2007. Locating proteins in the cell using TargetP, SignalP and related tools. *Nat Protoc,* 2**,** 953-71.

EMANUELSSON, O., NIELSEN, H. & VON HEIJNE, G. 1999. ChloroP, a neural network-based method for predicting chloroplast transit peptides and their cleavage sites. *Protein Sci,* 8**,** 978-84.

EMSLEY, P. & COWTAN, K. 2004. Coot: model-building tools for molecular graphics. *Acta Crystallogr D Biol Crystallogr,* 60**,** 2126-32.

EMSLEY, P., LOHKAMP, B., SCOTT, W. G. & COWTAN, K. 2010. Features and development of Coot. *Acta Crystallogr D Biol Crystallogr,* 66**,** 486-501.

FERRER-SUETA, G., MANTA, B., BOTTI, H., RADI, R., TRUJILLO, M. & DENICOLA, A. 2011. Factors affecting protein thiol reactivity and specificity in peroxide reduction. *Chem Res Toxicol,* 24**,** 434-50.

FRANKE, D., PETOUKHOV, M. V., KONAREV, P. V., PANJKOVICH, A., TUUKKANEN, A., MERTENS, H. D. T., KIKHNEY, A. G., HAJIZADEH, N. R., FRANKLIN, J. M., JEFFRIES, C. M. & SVERGUN, D. I. 2017. ATSAS 2.8: a comprehensive data analysis suite for small-angle scattering from macromolecular solutions. *J Appl Crystallogr,* 50**,** 1212-1225.

GAMIZ-ARCO, G., RISSO, V. A., CANDEL, A. M., INGLES-PRIETO, A., ROMERO-ROMERO, M. L., GAUCHER, E. A., GAVIRA, J. A., IBARRA-MOLERO, B. & SANCHEZ-RUIZ, J. M. 2019. Non-conservation of folding rates in the thioredoxin family reveals degradation of ancestral unassisted-folding. *Biochem J*.

GLEASON, F. K. & HOLMGREN, A. 1981. Isolation and characterization of thioredoxin from the cyanobacterium, Anabaena sp. *J Biol Chem,* 256**,** 8306-9.

GONZALEZ PORQUE, P., BALDESTEN, A. & REICHARD, P. 1970. Purification of a thioredoxin system from yeast. *J Biol Chem,* 245**,** 2363-70.

GREETHAM, D., VICKERSTAFF, J., SHENTON, D., PERRONE, G. G., DAWES, I. W. & GRANT, C. M. 2010. Thioredoxins function as deglutathionylase enzymes in the yeast Saccharomyces cerevisiae. *BMC Biochem,* 11**,** 3.

GRONENBORN, A. M., CLORE, G. M., LOUIS, J. M. & WINGFIELD, P. T. 1999. Is human thioredoxin monomeric or dimeric? *Protein Sci,* 8**,** 426-9.

GURRIERI, L., DEL GIUDICE, A., DEMITRI, N., FALINI, G., PAVEL, N. V., ZAFFAGNINI, M., POLENTARUTTI, M., CROZET, P., MARCHAND, C. H., HENRI, J., TROST, P., LEMAIRE, S. D., SPARLA, F. & FERMANI, S. 2019. Arabidopsis and Chlamydomonas phosphoribulokinase crystal structures complete the redox structural proteome of the Calvin-Benson cycle. *Proc Natl Acad Sci U S A,* 116**,** 8048-8053.

GUTLE, D. D., RORET, T., MULLER, S. J., COUTURIER, J., LEMAIRE, S. D., HECKER, A., DHALLEINE, T., BUCHANAN, B. B., RESKI, R., EINSLE, O. & JACQUOT, J. P. 2016. Chloroplast FBPase and SBPase are thioredoxin-linked enzymes with similar architecture but different evolutionary histories. *Proc Natl Acad Sci U S A,* 113**,** 6779-84.

HALL, D. E., BALDESTEN, A., HOLMGREN, A. & REICHARD, P. 1971. Yeast thioredoxin. Amino-acid sequence around the active-center disulfide of thioredoxin I and II. *Eur J Biochem,* 23**,** 328-35.

HANSCHMANN, E. M., GODOY, J. R., BERNDT, C., HUDEMANN, C. & LILLIG, C. H. 2013. Thioredoxins, glutaredoxins, and peroxiredoxins--molecular mechanisms and health significance: from cofactors to antioxidants to redox signaling. *Antioxid Redox Signal,* 19**,** 1539-605.

HIRASAWA, M., SCHURMANN, P., JACQUOT, J. P., MANIERI, W., JACQUOT, P., KERYER, E., HARTMAN, F. C. & KNAFF, D. B. 1999. Oxidation-reduction properties of chloroplast thioredoxins, ferredoxin:thioredoxin reductase, and thioredoxin f-regulated enzymes. *Biochemistry,* 38**,** 5200-5.

HOLMGREN, A. 1968. Thioredoxin. 6. The amino acid sequence of the protein from escherichia coli B. *Eur J Biochem,* 6**,** 475-84.

HOLMGREN, A., BUCHANAN, B. B. & WOLOSIUK, R. A. 1977. Photosynthetic regulatory protein from rabbit liver is identical with thioredoxin. *FEBS Lett,* 82**,** 351-4.

HOLMGREN, A. & MORGAN, F. J. 1976. Enzyme reduction of disulfide bonds by thioredoxin. The reactivity of disulfide bonds in human choriogonadotropin and its subunits. *Eur J Biochem,* 70**,** 377-83.

HUANG, C., YU, Q. B., LV, R. H., YIN, Q. Q., CHEN, G. Y., XU, L. & YANG, Z. N. 2013. The reduced plastid-encoded polymerase-dependent plastid gene expression leads to the delayed greening of the Arabidopsis fln2 mutant. *PLoS One,* 8**,** e73092.

HUPPE, H. C. & BUCHANAN, B. B. 1989. Activation of a chloroplast type of fructose bisphosphatase from Chlamydomonas reinhardtii by light-mediated agents. *Z Naturforsch C J Biosci,* 44**,** 487-94.

INGLES-PRIETO, A., IBARRA-MOLERO, B., DELGADO-DELGADO, A., PEREZ-JIMENEZ, R., FERNANDEZ, J. M., GAUCHER, E. A., SANCHEZ-RUIZ, J. M. & GAVIRA, J. A. 2013. Conservation of protein structure over four billion years. *Structure,* 21**,** 1690-7.

JACQUOT, J. P., EKLUND, H., ROUHIER, N. & SCHURMANN, P. 2009. Structural and evolutionary aspects of thioredoxin reductases in photosynthetic organisms. *Trends Plant Sci,* 14**,** 336-43.

KANG, Z., QIN, T. & ZHAO, Z. 2019. Thioredoxins and thioredoxin reductase in chloroplasts: A review. *Gene,* 706**,** 32-42.

KELLEY, L. A., MEZULIS, S., YATES, C. M., WASS, M. N. & STERNBERG, M. J. 2015. The Phyre2 web portal for protein modeling, prediction and analysis. *Nat Protoc,* 10**,** 845-58.

KELLEY, R. F. & RICHARDS, F. M. 1987. Replacement of proline-76 with alanine eliminates the slowest kinetic phase in thioredoxin folding. *Biochemistry,* 26**,** 6765-74.

KONIG, J., MUTHURAMALINGAM, M. & DIETZ, K. J. 2012. Mechanisms and dynamics in the thiol/disulfide redox regulatory network: transmitters, sensors and targets. *Curr Opin Plant Biol,* 15**,** 261-8.

KULCZYK, A. W., MOELLER, A., MEYER, P., SLIZ, P. & RICHARDSON, C. C. 2017. Cryo-EM structure of the replisome reveals multiple interactions coordinating DNA synthesis. *Proc Natl Acad Sci U S A,* 114**,** E1848-E1856.

LANCELIN, J. M., GUILHAUDIS, L., KRIMM, I., BLACKLEDGE, M. J., MARION, D. & JACQUOT, J. P. 2000. NMR structures of thioredoxin m from the green alga Chlamydomonas reinhardtii. *Proteins,* 41**,** 334-49.

LEE, S., KIM, S. M. & LEE, R. T. 2013. Thioredoxin and thioredoxin target proteins: from molecular mechanisms to functional significance. *Antioxid Redox Signal,* 18**,** 1165-207.

LEGRAND, P. 2017. XDSME: XDS Made Easier.

LEMAIRE, S. D., GUILLON, B., LE MARECHAL, P., KERYER, E., MIGINIAC-MASLOW, M. & DECOTTIGNIES, P. 2004. New thioredoxin targets in the unicellular photosynthetic eukaryote Chlamydomonas reinhardtii. *Proc Natl Acad Sci U S A,* 101**,** 7475-80.

LEMAIRE, S. D., MICHELET, L., ZAFFAGNINI, M., MASSOT, V. & ISSAKIDIS-BOURGUET, E. 2007. Thioredoxins in chloroplasts. *Curr Genet,* 51**,** 343-65.

LEMAIRE, S. D., TEDESCO, D., CROZET, P., MICHELET, L., FERMANI, S., ZAFFAGNINI, M. & HENRI, J. 2018. Crystal Structure of Chloroplastic Thioredoxin f2 from Chlamydomonas reinhardtii Reveals Distinct Surface Properties. *Antioxidants (Basel),* 7.

LEMASTER, D. M., SPRINGER, P. A. & UNKEFER, C. J. 1997. The role of the buried aspartate of Escherichia coli thioredoxin in the activation of the mixed disulfide intermediate. *J Biol Chem,* 272**,** 29998-30001.

LESLEY, S. A. & WILSON, I. A. 2005. Protein production and crystallization at the joint center for structural genomics. *J Struct Funct Genomics,* 6**,** 71-9.

LIEBTHAL, M., MAYNARD, D. & DIETZ, K. J. 2018. Peroxiredoxins and Redox Signaling in Plants. *Antioxid Redox Signal,* 28**,** 609-624.

LILLIG, C. H. & HOLMGREN, A. 2007. Thioredoxin and related molecules--from biology to health and disease. *Antioxid Redox Signal,* 9**,** 25-47.

MARCHAND, C. H., FERMANI, S., ROSSI, J., GURRIERI, L., TEDESCO, D., HENRI, J., SPARLA, F., TROST, P., LEMAIRE, S. D. & ZAFFAGNINI, M. 2019. Structural and Biochemical Insights into the Reactivity of Thioredoxin h1 from Chlamydomonas reinhardtii. *Antioxidants (Basel),* 8.

MARRI, L., ZAFFAGNINI, M., COLLIN, V., ISSAKIDIS-BOURGUET, E., LEMAIRE, S. D., PUPILLO, P., SPARLA, F., MIGINIAC-MASLOW, M. & TROST, P. 2009. Prompt and easy activation by specific thioredoxins of calvin cycle enzymes of Arabidopsis thaliana associated in the GAPDH/CP12/PRK supramolecular complex. *Mol Plant,* 2**,** 259-69.

MCCOY, A. J., GROSSE-KUNSTLEVE, R. W., ADAMS, P. D., WINN, M. D., STORONI, L. C. & READ, R. J. 2007. Phaser crystallographic software. *J Appl Crystallogr,* 40**,** 658-674.

MENCHISE, V., CORBIER, C., DIDIERJEAN, C., SAVIANO, M., BENEDETTI, E., JACQUOT, J. P. & AUBRY, A. 2001. Crystal structure of the wild-type and D30A mutant thioredoxin h of Chlamydomonas reinhardtii and implications for the catalytic mechanism. *Biochem J,* 359**,** 65-75.

MICHELET, L., ZAFFAGNINI, M., MARCHAND, C., COLLIN, V., DECOTTIGNIES, P., TSAN, P., LANCELIN, J. M., TROST, P., MIGINIAC-MASLOW, M., NOCTOR, G. & LEMAIRE, S. D. 2005. Glutathionylation of chloroplast thioredoxin f is a redox signaling mechanism in plants. *Proc Natl Acad Sci U S A,* 102**,** 16478-83.

MICHELET, L., ZAFFAGNINI, M., MASSOT, V., KERYER, E., VANACKER, H., MIGINIAC-MASLOW, M., ISSAKIDIS-BOURGUET, E. & LEMAIRE, S. D. 2006. Thioredoxins, glutaredoxins, and glutathionylation: new crosstalks to explore. *Photosynth Res,* 89**,** 225-45.

MICHELET, L., ZAFFAGNINI, M., MORISSE, S., SPARLA, F., PEREZ-PEREZ, M. E., FRANCIA, F., DANON, A., MARCHAND, C. H., FERMANI, S., TROST, P. & LEMAIRE, S. D. 2013. Redox regulation of the Calvin-Benson cycle: something old, something new. *Front Plant Sci,* 4**,** 470.

MORA-GARCIA, S., RODRIGUEZ-SUAREZ, R. & WOLOSIUK, R. A. 1998. Role of electrostatic interactions on the affinity of thioredoxin for target proteins. Recognition of chloroplast fructose-1, 6-bisphosphatase by mutant Escherichia coli thioredoxins. *J Biol Chem,* 273**,** 16273-80.

MORISSE, S., MICHELET, L., BEDHOMME, M., MARCHAND, C. H., CALVARESI, M., TROST, P., FERMANI, S., ZAFFAGNINI, M. & LEMAIRE, S. D. 2014. Thioredoxin-dependent redox regulation of chloroplastic phosphoglycerate kinase from Chlamydomonas reinhardtii. *J Biol Chem,* 289**,** 30012-24.

NAPOLITANO, S., REBER, R. J., RUBINI, M. & GLOCKSHUBER, R. 2019. Functional analyses of ancestral thioredoxins provide insights into their evolutionary history. *J Biol Chem,* 294**,** 14105-14118.

NAVROT, N., GELHAYE, E., JACQUOT, J. P. & ROUHIER, N. 2006. Identification of a new family of plant proteins loosely related to glutaredoxins with four CxxC motives. *Photosynth Res,* 89**,** 71-9.

NISHIZAWA, A. N. & BUCHANAN, B. B. 1981. Enzyme regulation in C4 photosynthesis. Purification and properties of thioredoxin-linked fructose bisphosphatase and sedoheptulose bisphosphatase from corn leaves. *J Biol Chem,* 256**,** 6119-26.

OJEDA, V., PEREZ-RUIZ, J. M. & CEJUDO, F. J. 2018. 2-Cys Peroxiredoxins Participate in the Oxidation of Chloroplast Enzymes in the Dark. *Mol Plant,* 11**,** 1377-1388.

OKEGAWA, Y. & MOTOHASHI, K. 2015. Chloroplastic thioredoxin m functions as a major regulator of Calvin cycle enzymes during photosynthesis in vivo. *Plant J,* 84**,** 900-13.

PALDE, P. B. & CARROLL, K. S. 2015. A universal entropy-driven mechanism for thioredoxin-target recognition. *Proc Natl Acad Sci U S A,* 112**,** 7960-5.

PAN, J. L. & BARDWELL, J. C. 2006. The origami of thioredoxin-like folds. *Protein Sci,* 15**,** 2217-27.

PEREZ-PEREZ, M. E., MATA-CABANA, A., SANCHEZ-RIEGO, A. M., LINDAHL, M. & FLORENCIO, F. J. 2009. A comprehensive analysis of the peroxiredoxin reduction system in the Cyanobacterium Synechocystis sp. strain PCC 6803 reveals that all five peroxiredoxins are thioredoxin dependent. *J Bacteriol,* 191**,** 7477-89.

PEREZ-PEREZ, M. E., MAURIES, A., MAES, A., TOURASSE, N. J., HAMON, M., LEMAIRE, S. D. & MARCHAND, C. H. 2017. The Deep Thioredoxome in Chlamydomonas reinhardtii: New Insights into Redox Regulation. *Mol Plant,* 10**,** 1107-1125.

PETOUKHOV, M. V., FRANKE, D., SHKUMATOV, A. V., TRIA, G., KIKHNEY, A. G., GAJDA, M., GORBA, C., MERTENS, H. D., KONAREV, P. V. & SVERGUN, D. I. 2012. New developments in the ATSAS program package for small-angle scattering data analysis. *J Appl Crystallogr,* 45**,** 342-350.

ROOS, G., FOLOPPE, N. & MESSENS, J. 2013. Understanding the pK(a) of redox cysteines: the key role of hydrogen bonding. *Antioxid Redox Signal,* 18**,** 94-127.

SCHROTER, Y., STEINER, S., MATTHAI, K. & PFANNSCHMIDT, T. 2010. Analysis of oligomeric protein complexes in the chloroplast sub-proteome of nucleic acid-binding proteins from mustard reveals potential redox regulators of plastid gene expression. *Proteomics,* 10**,** 2191-204.

SCHURMANN, P. & BUCHANAN, B. B. 2008. The ferredoxin/thioredoxin system of oxygenic photosynthesis. *Antioxid Redox Signal,* 10**,** 1235-74.

SETTERDAHL, A. T., CHIVERS, P. T., HIRASAWA, M., LEMAIRE, S. D., KERYER, E., MIGINIAC-MASLOW, M., KIM, S. K., MASON, J., JACQUOT, J. P., LONGBINE, C. C., DE LAMOTTE-GUERY, F. & KNAFF, D. B. 2003. Effect of pH on the oxidation-reduction properties of thioredoxins. *Biochemistry,* 42**,** 14877-84.

SEVILLA, F., CAMEJO, D., ORTIZ-ESPIN, A., CALDERON, A., LAZARO, J. J. & JIMENEZ, A. 2015. The thioredoxin/peroxiredoxin/sulfiredoxin system: current overview on its redox function in plants and regulation by reactive oxygen and nitrogen species. *J Exp Bot,* 66**,** 2945-55.

SUN, J., ZHENG, T., YU, J., WU, T., WANG, X., CHEN, G., TIAN, Y., ZHANG, H., WANG, Y., TERZAGHI, W., WANG, C. & WAN, J. 2017. TSV, a putative plastidic oxidoreductase, protects rice chloroplasts from cold stress during development by interacting with plastidic thioredoxin Z. *New Phytol,* 215**,** 240-255.

TARDIF, M., ATTEIA, A., SPECHT, M., COGNE, G., ROLLAND, N., BRUGIERE, S., HIPPLER, M., FERRO, M., BRULEY, C., PELTIER, G., VALLON, O. & COURNAC, L. 2012. PredAlgo: a new subcellular localization prediction tool dedicated to green algae. *Mol Biol Evol,* 29**,** 3625-39.

TARRAGO, L., LAUGIER, E., ZAFFAGNINI, M., MARCHAND, C., LE MARECHAL, P., ROUHIER, N., LEMAIRE, S. D. & REY, P. 2009. Regeneration mechanisms of Arabidopsis thaliana methionine sulfoxide reductases B by glutaredoxins and thioredoxins. *J Biol Chem,* 284**,** 18963-71.

TOLEDANO, M. B., DELAUNAY-MOISAN, A., OUTTEN, C. E. & IGBARIA, A. 2013. Functions and cellular compartmentation of the thioredoxin and glutathione pathways in yeast. *Antioxid Redox Signal,* 18**,** 1699-711.

TROST, P., FERMANI, S., MARRI, L., ZAFFAGNINI, M., FALINI, G., SCAGLIARINI, S., PUPILLO, P. & SPARLA, F. 2006. Thioredoxin-dependent regulation of photosynthetic glyceraldehyde-3-phosphate dehydrogenase: autonomous vs. CP12-dependent mechanisms. *Photosynth Res,* 89**,** 263-75.

VASEGHI, M. J., CHIBANI, K., TELMAN, W., LIEBTHAL, M. F., GERKEN, M., SCHNITZER, H., MUELLER, S. M. & DIETZ, K. J. 2018. The chloroplast 2-cysteine peroxiredoxin functions as thioredoxin oxidase in redox regulation of chloroplast metabolism. *Elife,* 7.

WANG, Y., WANG, Y., REN, Y., DUAN, E., ZHU, X., HAO, Y., ZHU, J., CHEN, R., LEI, J., TENG, X., ZHANG, Y., DI, W., ZHANG, X., GUO, X., JIANG, L., LIU, S., TIAN, Y., LIU, X., CHEN, L., WANG, H. & WAN, J. 2020. White Panicle2 encoding thioredoxin z, regulates plastid RNA editing by interacting with Multiple Organellar RNA Editing Factors in rice. *New Phytol*.

WATSON, W. H., POHL, J., MONTFORT, W. R., STUCHLIK, O., REED, M. S., POWIS, G. & JONES, D. P. 2003. Redox potential of human thioredoxin 1 and identification of a second dithiol/disulfide motif. *J Biol Chem,* 278**,** 33408-15.

WEDMANN, R., ONDERKA, C., WEI, S., SZIJARTO, I. A., MILJKOVIC, J. L., MITROVIC, A., LANGE, M., SAVITSKY, S., YADAV, P. K., TORREGROSSA, R., HARRER, E. G., HARRER, T., ISHII, I., GOLLASCH, M., WOOD, M. E., GALARDON, E., XIAN, M., WHITEMAN, M., BANERJEE, R. & FILIPOVIC, M. R. 2016. Improved tag-switch method reveals that thioredoxin acts as depersulfidase and controls the intracellular levels of protein persulfidation. *Chem Sci,* 7**,** 3414-3426.

WEICHSEL, A., GASDASKA, J. R., POWIS, G. & MONTFORT, W. R. 1996. Crystal structures of reduced, oxidized, and mutated human thioredoxins: evidence for a regulatory homodimer. *Structure,* 4**,** 735-51.

WIMMELBACHER, M. & BORNKE, F. 2014. Redox activity of thioredoxin z and fructokinase-like protein 1 is dispensable for autotrophic growth of Arabidopsis thaliana. *J Exp Bot,* 65**,** 2405-13.

WOLOSIUK, R. A. & BUCHANAN, B. B. 1978a. Activation of Chloroplast NADP-linked Glyceraldehyde-3-Phosphate Dehydrogenase by the Ferredoxin/Thioredoxin System. *Plant Physiol,* 61**,** 669-71.

WOLOSIUK, R. A. & BUCHANAN, B. B. 1978b. Regulation of chloroplast phosphoribulokinase by the ferredoxin/thioredoxin system. *Arch Biochem Biophys,* 189**,** 97-101.

YOKOCHI, Y., SUGIURA, K., TAKEMURA, K., YOSHIDA, K., HARA, S., WAKABAYASHI, K. I., KITAO, A. & HISABORI, T. 2019. Impact of key residues within chloroplast thioredoxin-f on recognition for reduction and oxidation of target proteins. *J Biol Chem*.

YOSHIDA, K., HARA, A., SUGIURA, K., FUKAYA, Y. & HISABORI, T. 2018. Thioredoxin-like2/2-Cys peroxiredoxin redox cascade supports oxidative thiol modulation in chloroplasts. *Proc Natl Acad Sci U S A,* 115**,** E8296-E8304.

YOSHIDA, K. & HISABORI, T. 2016. Two distinct redox cascades cooperatively regulate chloroplast functions and sustain plant viability. *Proc Natl Acad Sci U S A,* 113**,** E3967-76.

YOSHIDA, K. & HISABORI, T. 2017. Distinct electron transfer from ferredoxin-thioredoxin reductase to multiple thioredoxin isoforms in chloroplasts. *Biochem J,* 474**,** 1347-1360.

YOSHIDA, K., UCHIKOSHI, E., HARA, S. & HISABORI, T. 2019a. Thioredoxin-like2/2-Cys peroxiredoxin redox cascade acts as oxidative activator of glucose-6-phosphate dehydrogenase in chloroplasts. *Biochem J,* 476**,** 1781-1790.

YOSHIDA, K., YOKOCHI, Y. & HISABORI, T. 2019b. New Light on Chloroplast Redox Regulation: Molecular Mechanism of Protein Thiol Oxidation. *Front Plant Sci,* 10**,** 1534.

YUA, Q. B., MA, Q., KONG, M. M., ZHAO, T. T., ZHANG, X. L., ZHOU, Q., HUANG, C., CHONG, K. & YANG, Z. N. 2014. AtECB1/MRL7, a thioredoxin-like fold protein with disulfide reductase activity, regulates chloroplast gene expression and chloroplast biogenesis in Arabidopsis thaliana. *Mol Plant,* 7**,** 206-17.

ZAFFAGNINI, M., DE MIA, M., MORISSE, S., DI GIACINTO, N., MARCHAND, C. H., MAES, A., LEMAIRE, S. D. & TROST, P. 2016. Protein S-nitrosylation in photosynthetic organisms: A comprehensive overview with future perspectives. *Biochim Biophys Acta,* 1864**,** 952-66.

ZAFFAGNINI, M., FERMANI, S., MARCHAND, C. H., COSTA, A., SPARLA, F., ROUHIER, N., GEIGENBERGER, P., LEMAIRE, S. D. & TROST, P. 2019. Redox Homeostasis in Photosynthetic Organisms: Novel and Established Thiol-Based Molecular Mechanisms. *Antioxid Redox Signal,* 31**,** 155-210.

[figure and table legends]
Figure legends

Figure 1. Crystallographic structure of chloroplastic CrTRXz.
(A) Cartoon representation with helices 1-4 colored in cyan and strands 1-4 colored in magenta. Cysteines side chains are represented in sticks and highlighted with an asterisk. Residue numbering is in accordance with UniProt entry A8J0Q8-1. (B) 90° rotation around y-axis of A. (C) Electrostatic surface potential calculated with APBS (Baker et al., 2001). Electronegative surface is colored in red while electropositive surface is colored in blue. (D) 90° rotation around y-axis of C. (E) Conservation of surface residues as calculated with CONSURF colored from purple (most conserved) to blue (least conserved). (F) 90° rotation around y-axis of E. (G) B-factor representation. High b-factor are colored in red and low b-factor are colored in blue.

Figure 2. Redox site of CrTRXz.
Main chain is represented as cartoon. Side chains are represented as lines and colored according to atom type (blue=nitrogen, red=oxygen, yellow=sulfur). (A) Redox site ^{89}WCPGCL^{94} side chains are highlighted in sticks and labelled as three-letter code. C90 is located at the conserved nucleophile position. (B) Nucleophile D84 side chain is shown as sticks. The 6.4 Å carboxylate-thiol distance to C93 is drawn in broken line.

Figure 3. Thioredoxin z quaternary structure.
(A) Crystallographic dimer of CrTRXz represented in cartoon with reactive cysteines side chain in sticks. Chain A is colored in blue, chain B in green. (B) SAXS scattering curve log(I)=f(s) of batch 1 of CrTRXz in blue was fitted to the crystallographic monomeric model of CrTRXz in red. (C) Same experiment as B. with batch 2 of CrTRXz.

Figure 4. Structural comparison of plastidial TRX experimental structures.
Root mean square deviations (RMSD) between equivalent alpha carbons were calculated with PYMOL. (A) CrTRXz crystal structure (this study) represented in cartoon and colored from blue (amino-terminus) to red (amino-terminus). Cysteines sidechain are shown in sticks representation and highlighted with an asterisk. (B) Electrostatic surface potential of CrTRXz calculated with APBS (Baker et al., 2001). Electronegative surface is colored in red while electropositive surface is colored in blue. (C) CrTRXm nuclear magnetic resonance structure(Lancelin et al., 2000) (PDB identifier 1DBY) represented and colored as in A. (D) Electrostatic surface potential of CrTRXm calculated with APBS and colored as in B. (E) CrTRXf2 crystal structure (PDB entry 6I1C) represented and colored as in A. (F) Electrostatic surface potential calculated with APBS of CrTRXf2 and colored as in B.

Figure 5. Electrostatic surface of PHYRE2 (Kelley et al., 2015) homology-modelled TRXz protein partners.

(A) Connolly solvent exclusion surface of AtFLN1 residues 90-464 from the sequence of UniProt entry Q9M394 with Cysteines in yellow. (B) Electrostatic surface potential calculated with APBS. Electronegative surface is colored in red while electropositive surface is colored in blue (C) Connolly solvent exclusion surface of AtFLN2 205-557 from the sequence of UniProt entry F4I0K2 with Cysteines in yellow. (D) Electrostatic surface potential calculated with APBS and colored as in B. (E) Connolly solvent exclusion surface of AtMTR7 residues 195-312 from the sequence of UniProt entry F4JLC1 with Cysteines in yellow. (F) Electrostatic surface potential calculated with APBS and colored as in A.

Figure 6. Activation efficiency of CrTRXz, CrTRXf2, and CrTRXm on CrPRK.

Activation of oxidized CrPRK (5 µM) after 1 h incubation with increasing concentrations (0.5-50 µM) of CrTRXz (white bars), CrTRXf2 (light grey bars) and CrTRXm (dark grey bars) in presence of 0.2 mM DTT. TRX:PRK molar ratios (n:n) are indicated for each tested condition. Control sample (CTR, black bar) shows the activity after incubation with 0.2 mM DTT without TRXs. All the activities were normalized on fully activated PRK obtained after 4 h of reduction with 40 mM DTT. Data are reported as mean ± standard deviation (n=3).

Table 1. Crystallographic diffraction data and model statistics.
Statistics for the highest-resolution shell are reported in parentheses.
Supplementary figures

Supplementary figure 1. Sequence alignment of CrTRXz homologs.

Sequence alignment was performed by Clustal Omega with homologs from different species. Residues with more than 50% conservation are colored in red, strictly conserved residues are in white with a red background. Numbering is according to the sequence of TRXz from *Chlamydomonas reinhardtii*. TRX sequences were retrieved from UniprotKB database for the following species: *Chlamydomonas reinhardtii* (A8J0Q8), *Gonium pectorale* (A0A150FZQ6), *Tetrabaena socialis* (A0A2J7ZQ73), *Volvox carteri f. nagariensis* (D8TVT1), *Ostreococcus tauri* (A0A1Y5IIS5), *Arabidopsis thaliana* (Q9M7X9), *Synechocystis sp. PCC 6714* (A0A068MSG5), *Glycine max* (I1JW39).

Supplementary figure 2. CrTRX experimental structures.

(A) Side and top view of CrTRXz structure. CrTRXz is represented in cartoon colored in rainbow from N-terminus (blue) to C-terminus (red). Reactive cysteine side chains are represented in sticks. (B) CrTRXm in the same orientation, representation and coloration as A. (C) CrTRXf2 in the same orientation, representation and coloration as A. (D) Structural alignment of CrTRXf2, CrTRXm and CrTRXh structure colored in white on CrTRXz colored in green structure realized by PyMOL. RMSD of alignments are respectively 1.357 Å, 0.838 Å and 1.123 Å for CrTRXm, CrTRXf2 and CrTRXh.

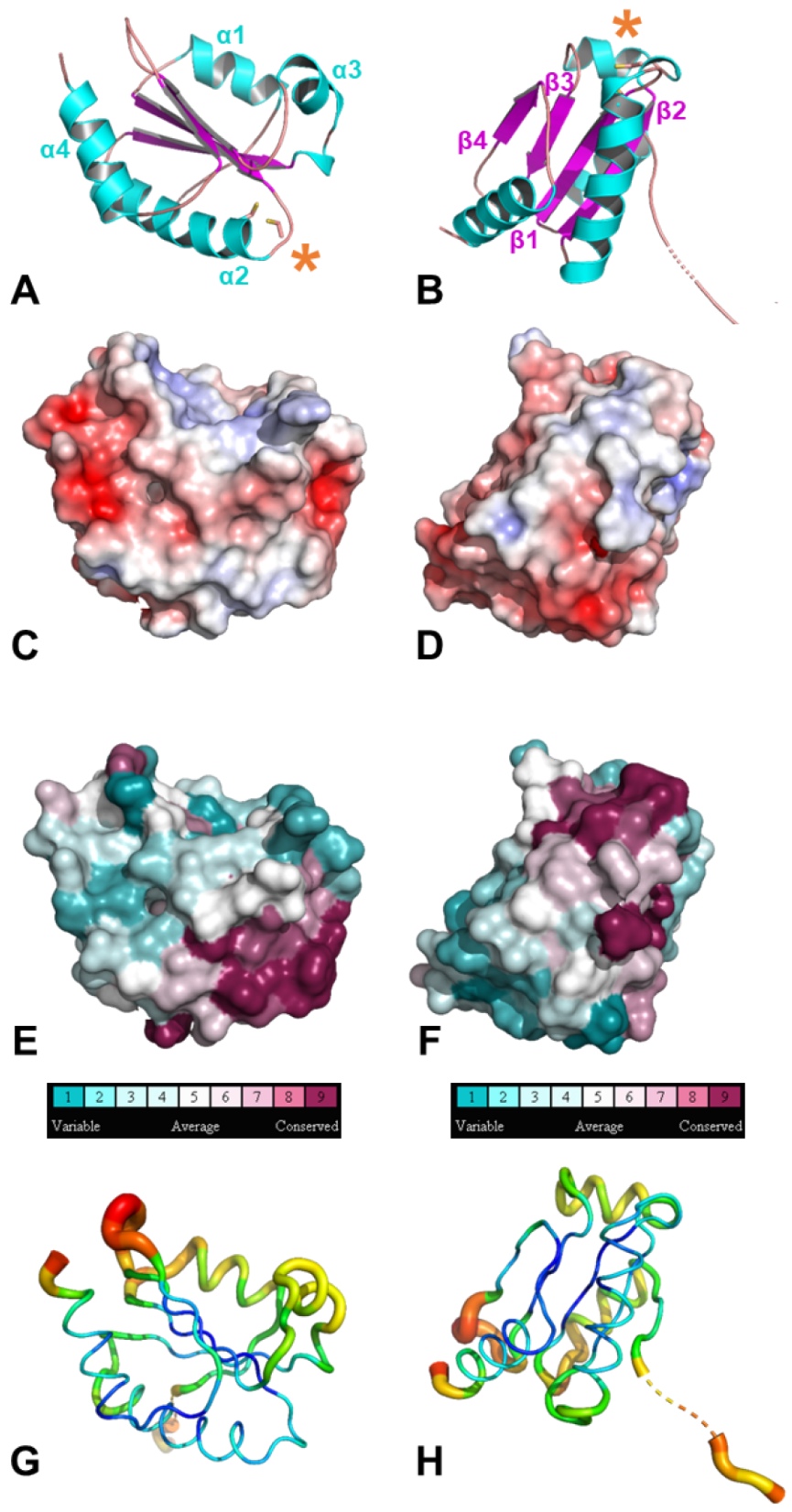Supplementary figure 3. CrTRXz size-exclusion chromatography.

High-pressure liquid chromatography profile over BioSEC3-300 column of (A) preparation 1 and (B) preparation 2 of CrTRZx. Globular calibration standards elute at 7.2 mL (670 kDa), 9.2 mL (158 kDa), 10.6 mL (44 kDa), 11.7 mL (17 kDa). Dead column volume is 6.5 mL and total column volume is 13.4 mL. TRXz peaks are pointed by green arrows.
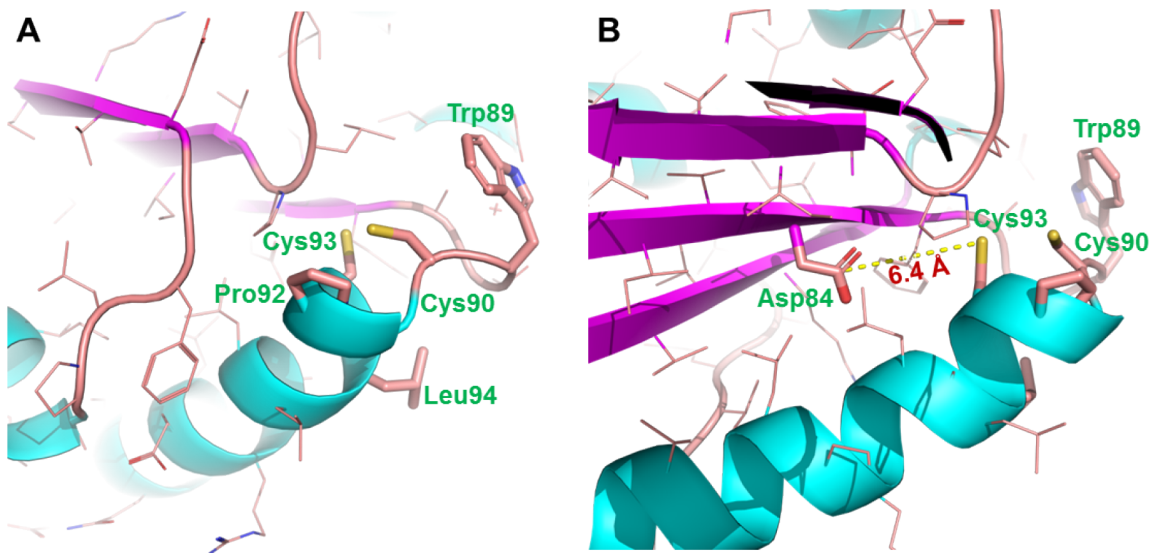
Supplementary figure 4. Comparison of homology models of *Arabidopsis thaliana* TRXz computed from sequence in entry Uniprot Q9M7X9 isoform 1 with the experimental structure of *Chlamydomonas reinhardtii* TRXz. Structures align with RMSD of 1.1-1.4 Å. Nucleophilic cysteines side chains are displayed as spheres with sulfur in gold. (A) *Arabidopsis thaliana* TRXz Swiss-model by homology with 50 template thioredoxins. (B) Experimental crystal structure of *Chlamydomonas reinhardtii* TRXz (this study). (C) *Arabidopsis thaliana* TRXz model from Phyre2 with confidence score=99/100 to an ortholog of 24% sequence identity. (D) Electrostatic potential of AtTRXz Swiss-model. (E) Electrostatic potential
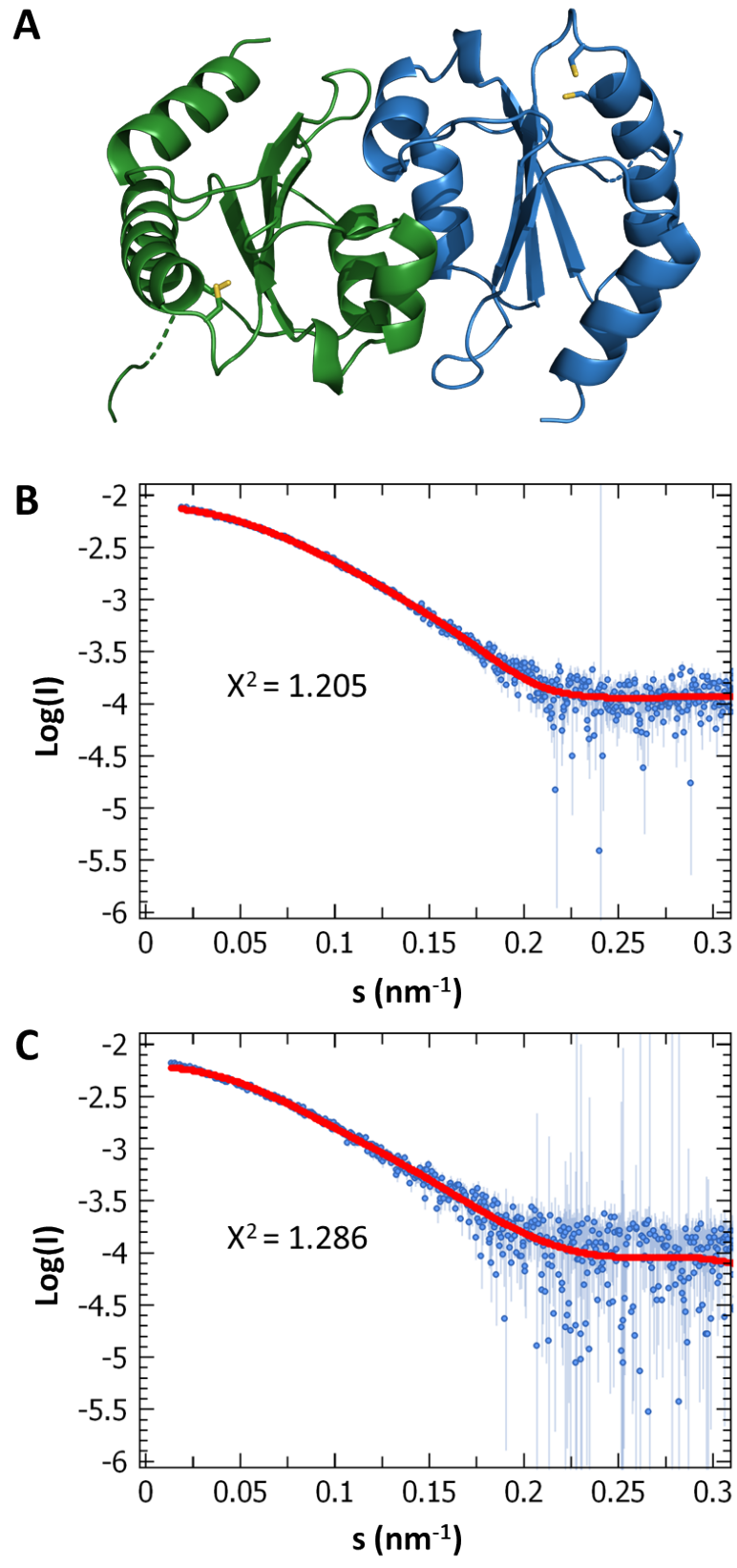
of CrTRXz crystal structure. (F) Electrostatic potential of AtTRXz Phyre2 model. Potential is colored from red (negative) to blue (positive).
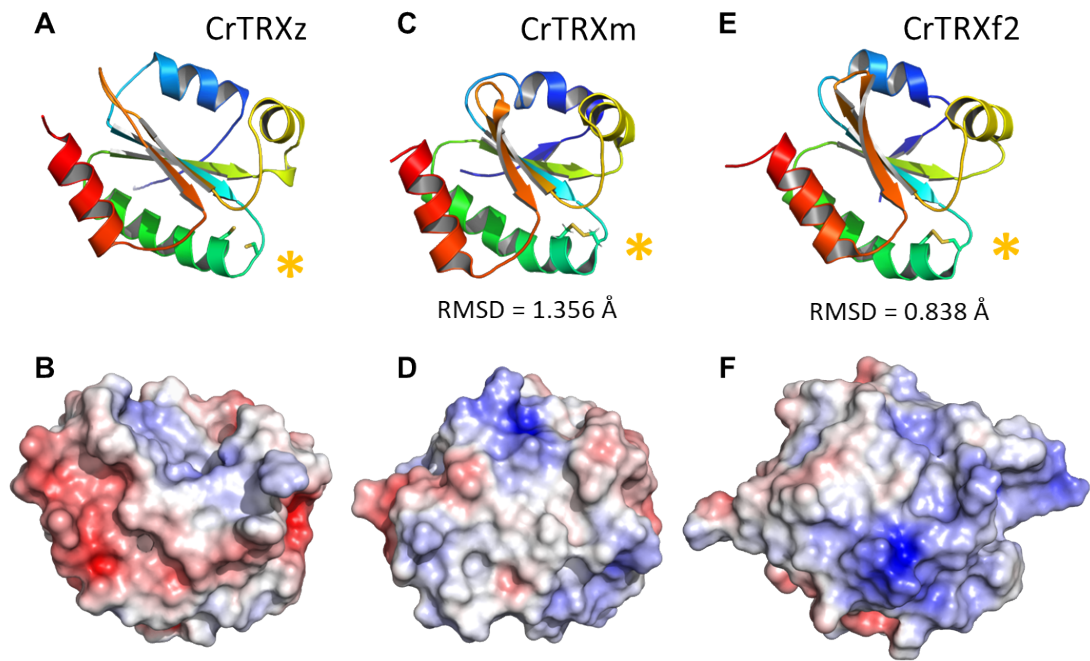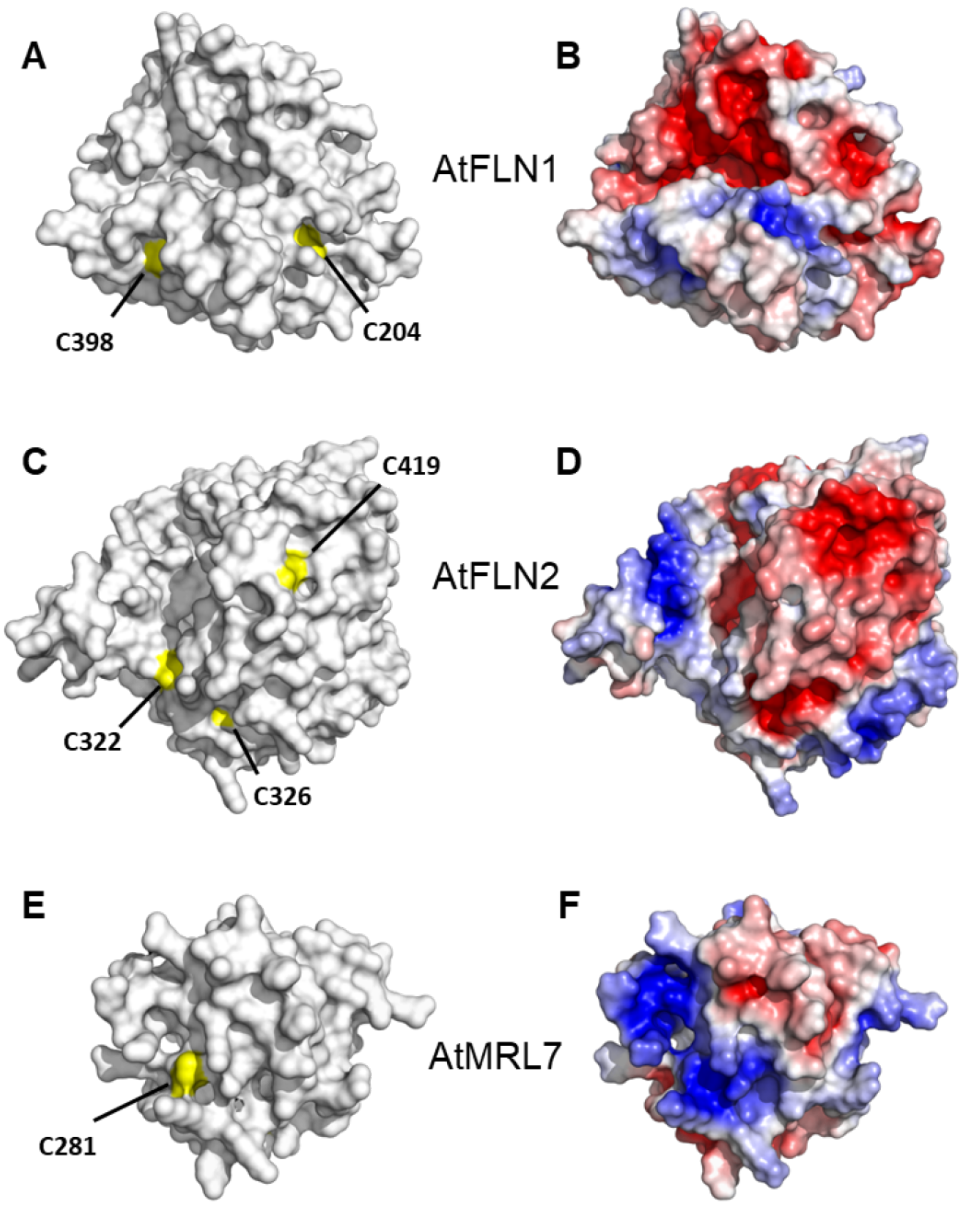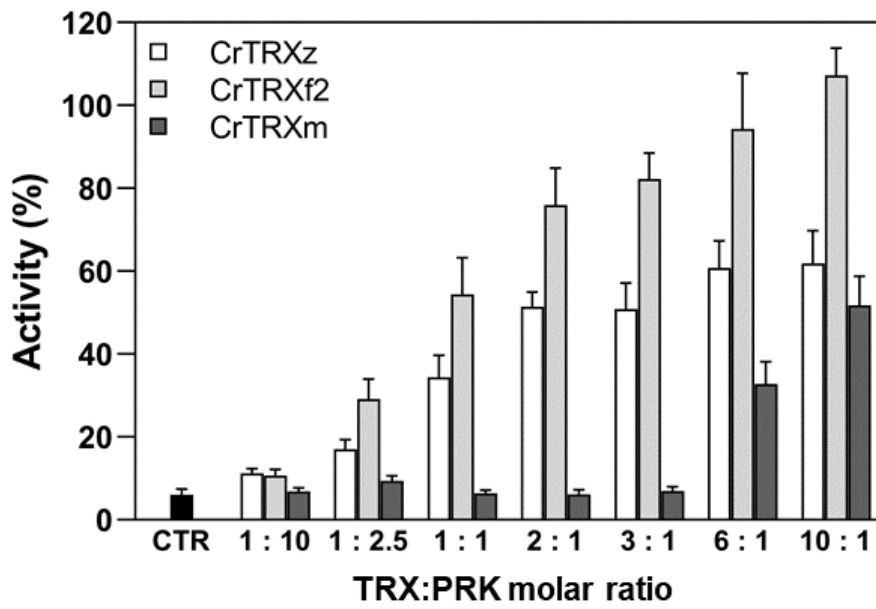
Table 1.

	CrTRXz
Resolution range	40.34 - 2.444 (2.532 - 2.444)
Space group	P 32 2 1
Unit cell	61.985 61.985 61.138 90 90 120
Total reflections	210020 (19582)
Unique reflections	5300 (485)
Multiplicity	39.6(38.0)
Completeness (%)	99.40 (94.17)
Mean I/sigma(I)	17.68 (1.29)
Wilson B-factor	65,65
R-merge	0.6065 (1.461)
R-meas	0.6145 (1.48)
R-pim	0.09769 (0.2389)
CC1/2	0.909 (0.792)
CC*	0.976 (0.94)
Reflections used in refinement	5269 (485)
Reflectione used for R-free	525 (36)
R-work	0.2296 (0.3471)
R-free	0.2335 (0.3213)
CC(work)	0.462 (0.009)
CC(free)	0.38(0.246)
Number of non-hydrogen atoms	865
macromolecules	864
solvent	1
Protein residues	113
RMS(bonds)	0,010
RMS(angles)	1,44
Ramachandran favored (%)	99,08
Ramachandran allowed (%)	0,92
Ramachandran outliers (%)	0,00
Rotamer outliers (%)	7,37
Clashscore	6,82
Average B-factor	70,15
macromolecules	70,19
solvent	30

Figure 1.

Figure 2. The Plant Journal Page 22 of 34

Figure 3.

A

B

$X^2 = 1.205$

Log(I)

s (nm^{-1})

C

$X^2 = 1.286$

Log(I)

s (nm^{-1})

Figure 4.   The Plant Journal   Page 24 of 34

A   CrTRXz

C   CrTRXm

RMSD = 1.356 Å

E   CrTRXf2

RMSD = 0.838 Å

B

D

F

Figure 5.

A   C398   C204

B   AtFLN1

C   C419   C322   C326

D   AtFLN2

E   C281

F   AtMRL7

Figure 6.

Table 1.

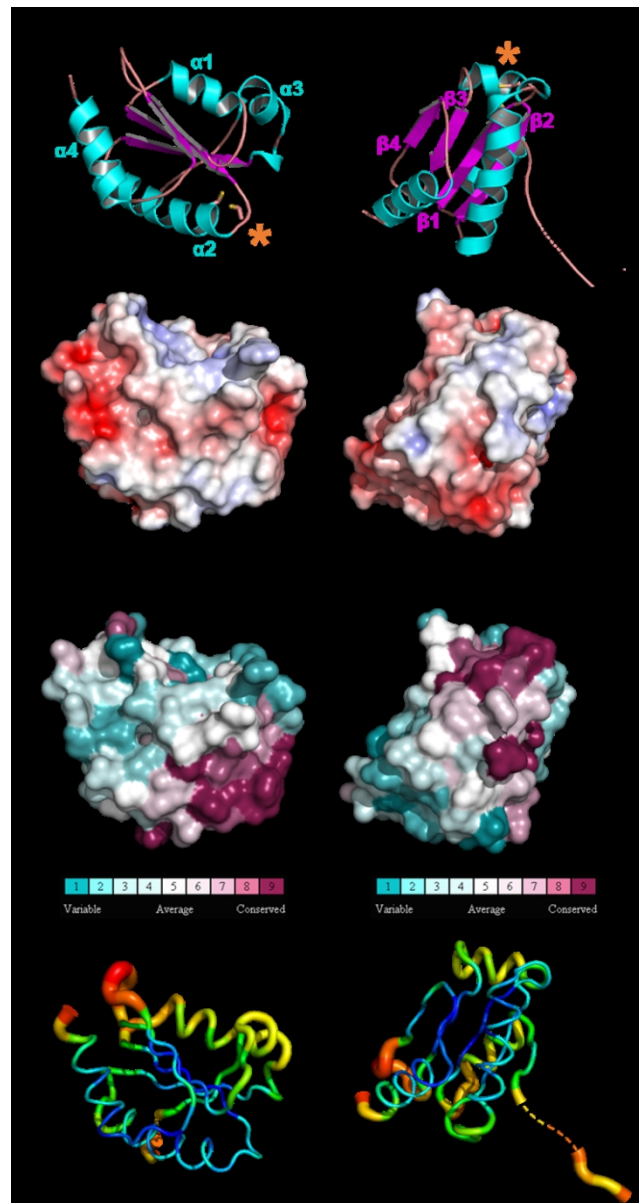|	CrTRXz
Resolution range	40.34 - 2.444 (2.532 - 2.444)
Space group	P 32 2 1
Unit cell	61.985 61.985 61.138 90 90 120
Total reflections	210020 (19582)
Unique reflections	5300 (485)
Multiplicity	39.6(38.0)
Completeness (%)	99.40 (94.17)
Mean I/sigma(I)	17.68 (1.29)
Wilson B-factor	65,65
R-merge	0.6065 (1.461)
R-meas	0.6145 (1.48)
R-pim	0.09769 (0.2389)
CC1/2	0.909 (0.792)
CC*	0.976 (0.94)
Reflections used in refinement	5269 (485)
Reflectione used for R-free	525 (36)
R-work	0.2296 (0.3471)
R-free	0.2335 (0.3213)
CC(work)	0.462 (0.009)
CC(free)	0.38(0.246)
Number of non-hydrogen atoms	865
macromolecules	864
solvent	1
Protein residues	113
RMS(bonds)	0,010
RMS(angles)	1,44
Ramachandran favored (%)	99,08
Ramachandran allowed (%)	0,92
Ramachandran outliers (%)	0,00
Rotamer outliers (%)	7,37
Clashscore	6,82
Average B-factor	70,15
macromolecules	70,19
solvent	30

Figure 1. Crystallographic structure of chloroplastic CrTRXz.
(A) Cartoon representation with helices 1-4 colored in cyan and strands 1-4 colored in magenta. Cysteines side chains are represented in sticks and highlighted with an asterisk. Residue numbering is in accordance with UniProt entry A8J0Q8-1. (B) 90° rotation around y-axis of A. (C) Electrostatic surface potential calculated with APBS [108]. Electronegative surface is colored in red while electropositive surface is colored in blue. (D) 90° rotation around y-axis of C. (E) Conservation of surface residues as calculated with CONSURF colored from purple (most conserved) to blue (least conserved). (F) 90° rotation around y-axis of E. (G) B-factor representation. High b-factor are colored in red and low b-factor are colored in blue.
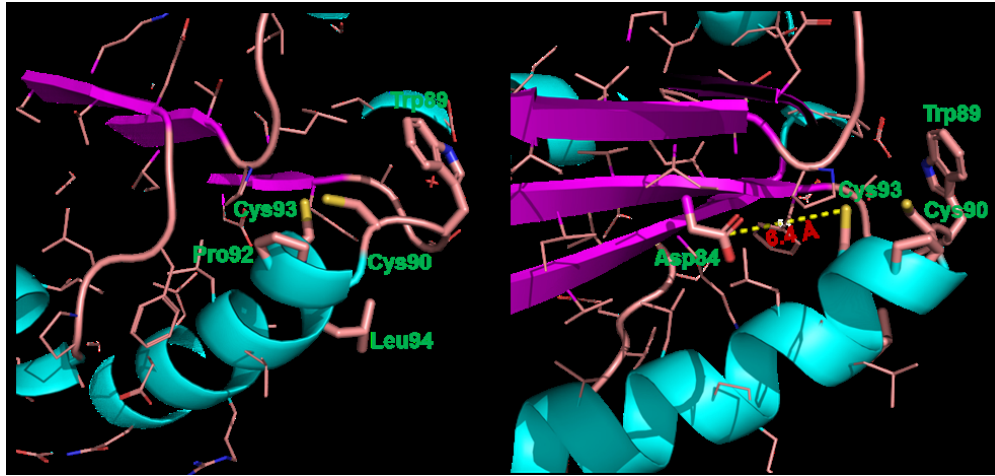
Figure 2. Redox site of CrTRXz.
Main chain is represented as cartoon. Side chains are represented as lines and colored according to atom type (blue=nitrogen, red=oxygen, yellow=sulfur). (A) Redox site 89WCPGCL94 side chains are highlighted in sticks and labelled as three-letter code. C90 is located at the conserved nucleophile position. (B) Nucleophile D84 side chain is shown as sticks. The 6.4 Å carboxylate-thiol distance to C93 is drawn in broken line.
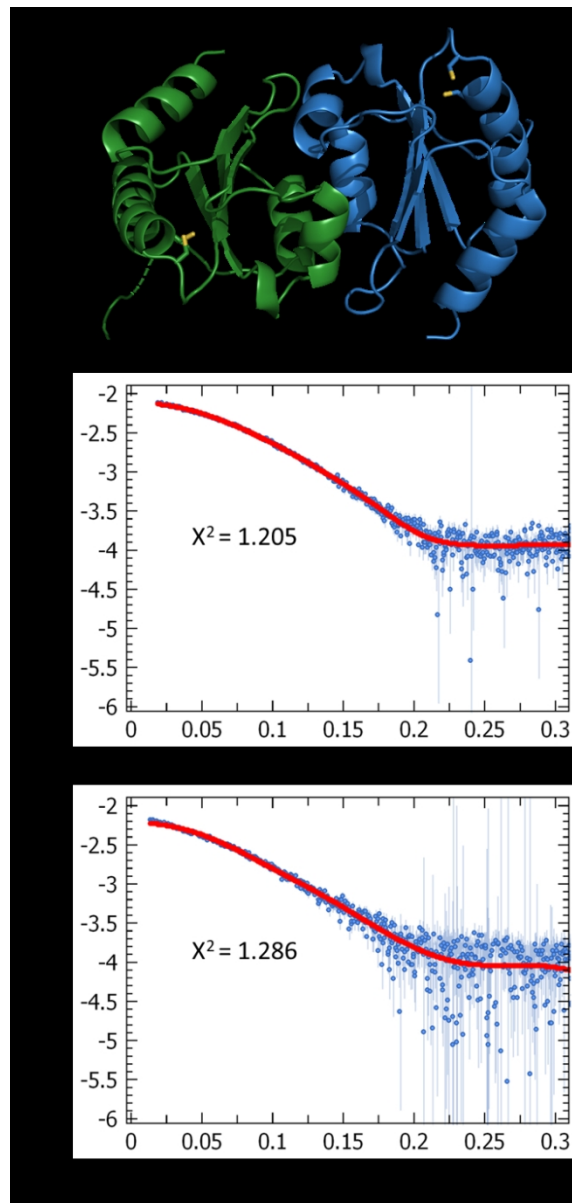
Figure 3. Thioredoxin z quaternary structure.
(A) Crystallographic dimer of CrTRXz represented in cartoon with reactive cysteines side chain in sticks. Chain A is colored in blue, chain B in green. (B) SAXS scattering curve log(I)=f(s) of batch 1 of CrTRXz in blue was fitted to the crystallographic monomeric model of CrTRXz in red. (C) Same experiment as B. with batch 2 of CrTRXz.
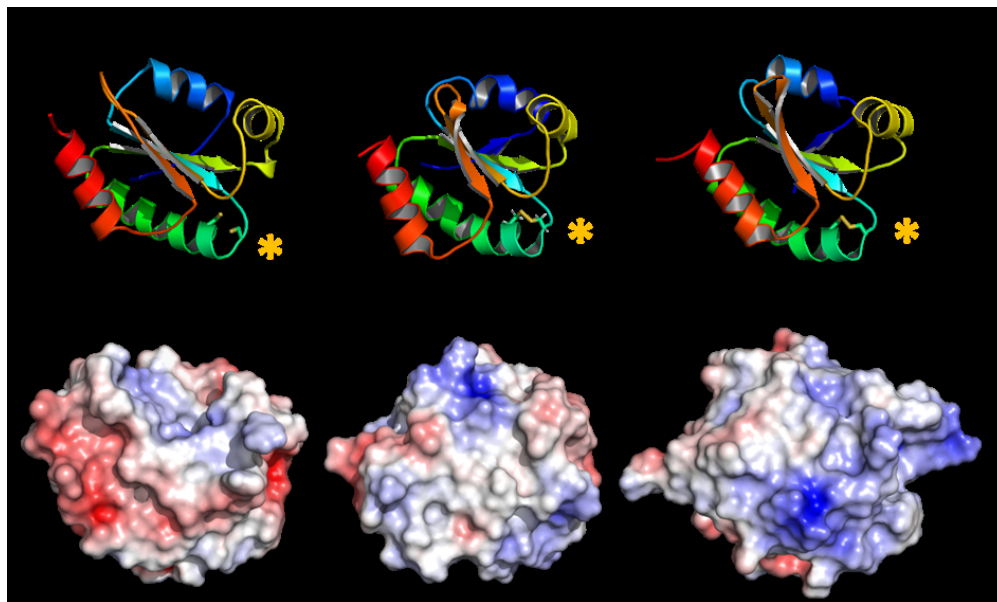
Figure 4. Structural comparison of plastidial TRX experimental structures.
Root mean square deviations (RMSD) between equivalent alpha carbons were calculated with PYMOL. (A) CrTRXz crystal structure (this study) represented in cartoon and colored from blue (amino-terminus) to red (amino-terminus). Cysteines sidechain are shown in sticks representation and highlighted with an asterisk. (B) Electrostatic surface potential of CrTRXz calculated with APBS [108]. Electronegative surface is colored in red while electropositive surface is colored in blue. (C) CrTRXm nuclear magnetic resonance structure[109] (PDB identifier 1DBY) represented and colored as in A. (D) Electrostatic surface potential of CrTRXm calculated with APBS and colored as in B. (E) CrTRXf2 crystal structure (PDB entry 6I1C) represented and colored as in A. (F) Electrostatic surface potential calculated with APBS of CrTRXf2 and colored as in B.
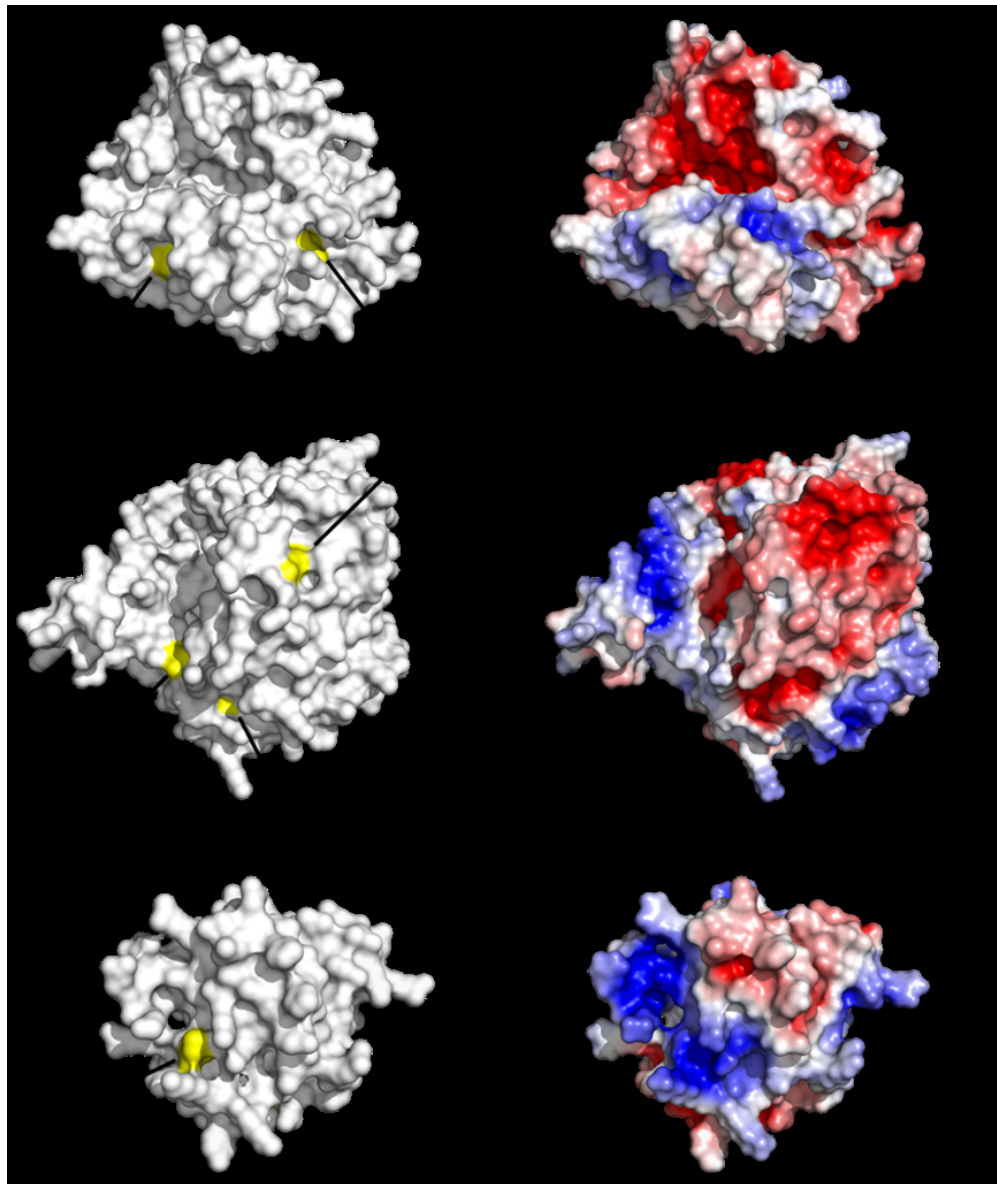
Figure 5. Electrostatic surface of PHYRE2 [87] homology-modelled TRXz protein partners.
(A) Connolly solvent exclusion surface of AtFLN1 residues 90-464 from the sequence of UniProt entry Q9M394 with Cysteines in yellow. (B) Electrostatic surface potential calculated with APBS. Electronegative surface is colored in red while electropositive surface is colored in blue (C) Connolly solvent exclusion surface of AtFLN2 205-557 from the sequence of UniProt entry F4I0K2 with Cysteines in yellow. (D) Electrostatic surface potential calculated with APBS and colored as in B. (E) Connolly solvent exclusion surface of AtMTR7 residues 195-312 from the sequence of UniProt entry F4JLC1 with Cysteines in yellow. (F) Electrostatic surface potential calculated with APBS and colored as in A.
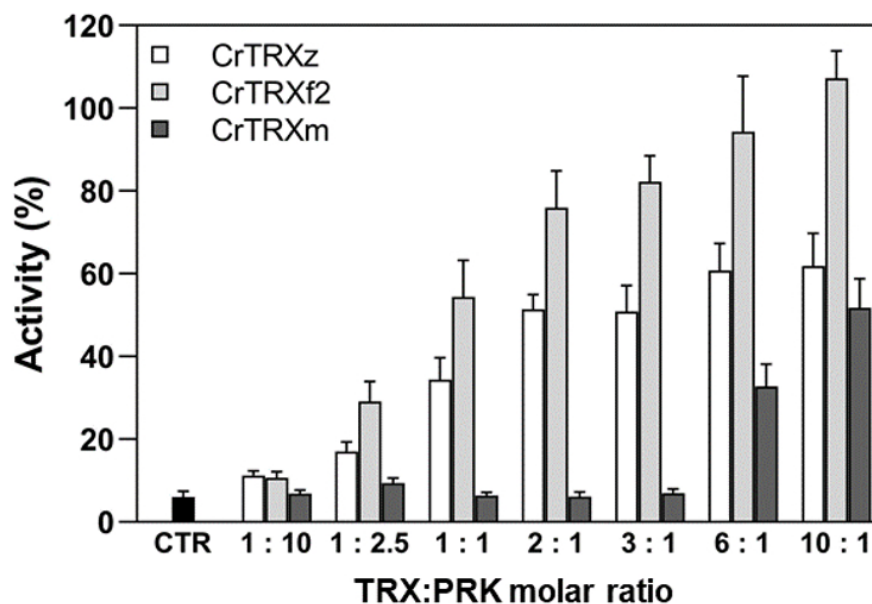
Figure 6. Activation efficiency of CrTRXz, CrTRXf2, and CrTRXm on CrPRK.
Activation of oxidized CrPRK (5 μM) after 1 h incubation with increasing concentrations (0.5-50 μM) of CrTRXz (white bars), CrTRXf2 (light grey bars) and CrTRXm (dark grey bars) in presence of 0.2 mM DTT. TRX:PRK molar ratios (n:n) are indicated for each tested condition. Control sample (CTR, black bar) shows the activity after incubation with 0.2 mM DTT without TRXs. All the activities were normalized on fully activated PRK obtained after 4 h of reduction with 40 mM DTT. Data are reported as mean ± standard deviation (n=3).

The high-resolution crystal structure of thioredoxin z from the model eukaryotic alga *Chlamydomonas reinhardtii* confirms that TRXz is generally structured as a canonical redox TRX but exposes a type-specific electronegative surfaces around its active site. TRXz ability to interact with its target proteins is determined by this surface and reveals a compatibility with Calvin-Benson phosphoribulokinase (PRK) that proved to be activated by TRXz *in vitro*. TRXz hence appears as a novel player of photosynthesis.